PHILOSOPHICAL TRANSACTIONS OF THE ROYAL SOCIETY A MATHEMATICAL, PHYSICAL & ENGINEERING SCIENCES

Strain Effects, Particularly in Phase Transitions

A. M. Bratkovsky, Volker Heine and E. K. H. Salje

Phil. Trans. R. Soc. Lond. A 1996 **354**, 2875-2896
doi: 10.1098/rsta.1996.0133

Strain effects, particularly in phase transitions

By A. M. Bratkovsky[1]†, Volker Heine[2] and E. K. H. Salje[3]

[1]*Department of Materials, University of Oxford, Oxford OX1 3PH, UK*
[2]*Cavendish Laboratory, Madingley Road, Cambridge CB3 0HE, UK*
[3]*Department of Earth Sciences, Downing Street, Cambridge CB2 3EQ, UK*

Recent progress in understanding kinetics of texturing during structural phase transitions with long-range strain interactions is reviewed. We analyse systems with elastically mediated interaction which due to its anisotropy and infinite range has a pronounced effect on kinetics and textures occurring during the phase transition. As a generic example the textures ('stripe' and 'tweed' phases) due to oxygen ordering in layered high-T_c cuprates (YBCO) are discussed.

An atomic ordering process in cell i generates a local stress field, which is propagated elastically to a distant cell j. The effective elastic interaction $J(R_{ij})$ at large distances can be broken into a highly anisotropic spatial part, defining a few 'soft' directions coinciding with the orientation of twin boundaries, and the so-called Zener interaction J_Z of infinite range. The spatial part of the interaction falls off $\propto 1/R_{ij}^3$ in ferroelastic and $\propto 1/R_{ij}^5$ in anti-ferroelastic materials, with corresponding differences of the properties of domain walls in these two cases.

We analyse the origin of tweed texture usually seen when a ferroelastic material is quenched through the transition temperature T_c, and under other conditions. It is argued that a dense mass of embryos of the ordered phase is present as thermodynamic fluctuations at temperatures well above T_c. These fluctuations control the length and width of the tweed microdomains observed after quenching. Further coarsening of the tweed towards a stripe texture proceeds via the creation of needle domains governed by the strains around right-angled domain walls. Unusual texture formation under sudden heating is discussed.

1. Introduction

The structure of solids is defined by the size and packing of atoms and groups of atoms. Examples are the shapes of rather rigid units such as BX_4^{2-}, NO_2^-, or CO_3^{2-} ions or the C_6H_5 phenyl group (Etxebarria *et al.* 1990, 1992; Michel & Rowe 1985; Ortiz-Lopez & Luty 1988; Benkert *et al.* 1987), and the linking of also rather rigid SiO_4 tetrahedra in framework silicate structures (Putnis 1992) or octahedra in perovskites (Powell & Gerlach 1989). The same packing and linking principle applies, by extension, in structural phase transitions of either the displacive type or atomic ordering or orientation of the units mentioned previously (Dove *et al.* 1992, 1993; Giddy *et al.* 1993; Tautz *et al.* 1991; Vallade *et al.* 1992). Intimately related to this

† Present address: Hewlett-Packard Laboratories, 3500 Deer Creek Road, Bldg. 26, Palo Alto, CA 94304-1392, USA.

Phil. Trans. R. Soc. Lond. A (1996) **354**, 2875–2896
Printed in Great Britain

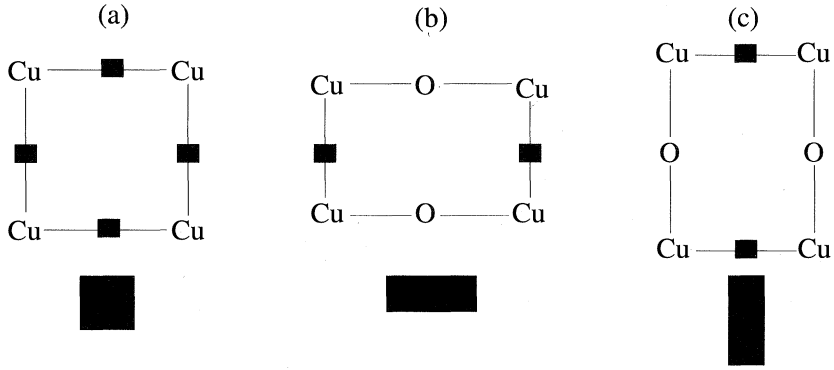

Figure 1. Schematic view of the Cu(1)-O plane of YBCO: (a) high-temperature tetragonal phase, oxygen atoms populate equally all positions denoted by heavy dots; (b, c) low-temperature orthorhombic phase, oxygen atoms mainly occupy two preferential configurations that results in a spontaneous strain.

general class of phenomena are the metastable tweed-like textures formed in diverse materials undergoing a structural phase transition, e.g. the tetragonal to orthorhombic transition in YBCO lightly doped by three-dimensional impurities (Schmahl *et al.* 1989; Van Tandeloo *et al.* 1987). Tweed texture is usually seen after cooling through the transition temperature T_c and consists of long thin microdomains, which coarsen with time. The involvement of long-range elastic forces is well-known (Marais *et al.* 1991*a*; Bratkovsky *et al.* 1994*a*, *b*, *c*; Wen *et al.* 1981). Sometimes the strain energy accounts for up to 50% of the enthalpy of the phase transformation (Salje *et al.* 1985).

We shall further explore the strain effects in the context of phase transformations, but phenomena where a strain mediated interaction is important are much wider. The strain fields are, for instance, generated by, for example, defect or impurity which could be relieved near a free surface (Tersoff 1995), or during a stick–slip process in a grain boundary sliding, or dislocation movement which releases strain when rebonding occurs.

Unfortunately, the role of strain fields is largely ignored in the current literature, perhaps partially because of the mathematical complexity needed in the description of strain. However, the study of strain effects is now coming to the fore, as shown by this volume. Here we shall limit ourselves to ferroelastic second-order phase transitions.

The physical picture of strain effects is clear: when atomic ordering takes place in one unit cell of the crystal or when one unit rotates at position $\boldsymbol{R}_i$, it inevitably pulls or pushes atoms or/and whole structural units; i.e. it creates a local displacement field. This field then displaces adjacent atoms and hence it creates a wider local displacement field. Hence any distortion propagates elastically to distant points $\boldsymbol{R}_j$ of the crystal via a knock-on effect. The resultant local strain at $\boldsymbol{R}_j$ then acts as an ordering force there. In other words, there is an indirect ordering interaction $J(\boldsymbol{R}_{ij})$ in the material mediated purely by strain.

Mesoscopic textures (e.g. tweed), frequently accompanying phase transitions in ferroelastic materials, are clearly related to elastic forces because their characteristic length scales are much larger than the lattice spacing (with oxygen-deficient YBCO as a typical example (Schmahl *et al.* 1989; Van Tendeloo *et al.* 1987; Salje & Parlinski 1991; Semenovskaya & Khachaturyan 1991, 1992)). This case is a useful paradigm

due to relative simplicity of oxygen ordering (figure 1). Tweed texture presents itself as a cross-hatched fine pattern of microdomains where the overall degree of order is small due to abundance of domain walls, but each microdomain is well ordered inside. We show in figure 2 an experimental picture of a tweed in feldspar together with a schematic picture of microdomains.

The strain mediated interaction is anisotropic and it triggers the tweed formation below critical temperature in the presence of any inhomogeneity. In the present study the thermal fluctuations in a perfect system drive the tweed formation, but similar tweed patterns can also be due to point defects, sudden heating, inhomogeneities or instant releases of pressure.

Textures, and tweed texture in particular, are not only ubiquitous and can be produced in many ways, but they also play an important role in materials properties like flux pinning in high-T_c superconductors.

Our paper is arranged as follows. In the following section we consider the nature of local strain and strain coupling, then we analyse its effect on ordering kinetics and texture formation in § 3 and go over to a discussion of the origin of tweed texture in § 4. The effect of sudden heating, inhomogeneities on ferroelastic material are described in § 5 and conclusions are given in § 6.

2. The nature of local strain and the 'effective exchange energy'

We consider structures of solids which are largely determined by packing together atoms, molecules or structural units such as BX_4 tetrahedra or BX_6 octahedra, or by linking such units via shared corner atoms into a framework structure, e.g. perovskite. Hence in a structural phase transition the atomic ordering occurring in one unit cell will exert stresses locally on the surrounding material. The resultant strain field propagates elastically to distant parts of a sample and interacts with the local ordering there. There is therefore an indirect coupling $J(\boldsymbol{R}_{ij})$ between the ordering in cells i and j mediated by local strain (figure 3).

We have studied the indirect coupling $J(\boldsymbol{R}_{ij})$ theoretically and by computer simulation: the form of $J(\boldsymbol{R}_i)$ and its Fourier transform $J_{\boldsymbol{k}}$, particularly their anisotropy and long-range behaviour (Bratkovsky *et al.* 1995), with application to the kinetics of ordering and the formation of metastable textures of microdomains (Bratkovsky *et al.* 1994*b*, *c*), and fluctuations (Bratkovsky *et al.* 1994*a*), especially the tweed texture found in a wide variety of materials (Khachaturyan 1983; Tanner *et al.* 1982; Salje 1993*a*; Bratkovsky *et al.* 1994*c*).

Let us first discuss some general features of $J(\boldsymbol{R})$. Perhaps the most important characteristic of $J(\boldsymbol{R})$ is its symmetry. For example in figure 3 the net interaction $J(\boldsymbol{R}_{ij})$ is ferroelastic and the local deformation is a shear e_{xy}. In figure 4*a* local ordering at $\boldsymbol{R}_i$ creates a force field that does not have the symmetry of a shear and figures 4*a*, *b* show that the ordering is ferroelastic and antiferroelastic, respectively. Ferroelastic local ordering (figure 3) is analogous to that of the usual force dipole (Eshelby 1956) and results in an anisotropic strain field falling off as $J_{\mathrm{F}}(\boldsymbol{R}) \propto 1/R^3$. In the antiferroelastic case the decay of interaction is necessarily stronger, $J_{\mathrm{AF}}(\boldsymbol{R}) \propto 1/R^5$. At large distances we obtain broadly speaking the following asymptotic forms (Bratkovsky *et al.* 1995):

(i) ferroelastic case (F)

$$J(\boldsymbol{R}) = \frac{A_4 Y_{4m}(\theta,\phi) + A_2 Y_{2m}(\theta,\phi) + A_6 Y_{6m}(\theta,\phi)}{R^3} + J_{\mathrm{Z}}, \tag{2.1}$$

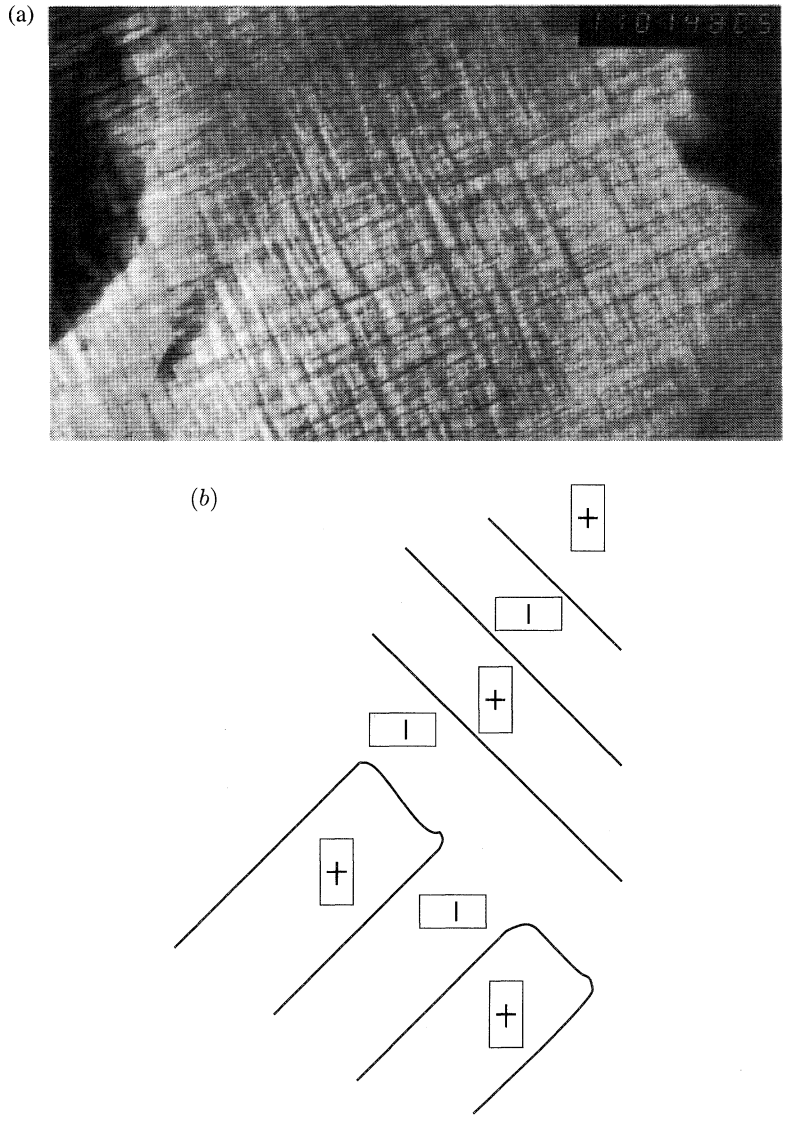

Figure 2. (*a*) Microstructure of Co-doped $YBa_2(Cu,Co)_3O_7$. Scale: the black label insert is 0.2 μm long (photograph by courtesy of A. Putnis, Cambridge). (*b*) Tweed texture in Co-doped YBCO (schematic). The domains with opposite spontaneous strains are shown to form a characteristic cross-hatched domain pattern.

where $J_Z = Z/N$ is the Zener–Eshelby constant term due to image forces on a free surface (Zener 1948; Eshelby 1956);

(ii) antiferroelastic case (AF)

$$J(\boldsymbol{R}) = \frac{A_4 Y_{4m}(\theta,\phi) + A_2 Y_{2m}(\theta,\phi) + A_6 Y_{6m}(\theta,\phi)}{R^5}. \tag{2.2}$$

Here Y_{lm} represents some appropriate spherical harmonic of order l, and the Y_{4m} term has been put first because it is usually the dominant one.

The most anomalous part of equation (2.1) is the term J_Z, which is constant, i.e. it has infinite range. We note that ferroelastic ordering in a single unit cell contributes $\propto$

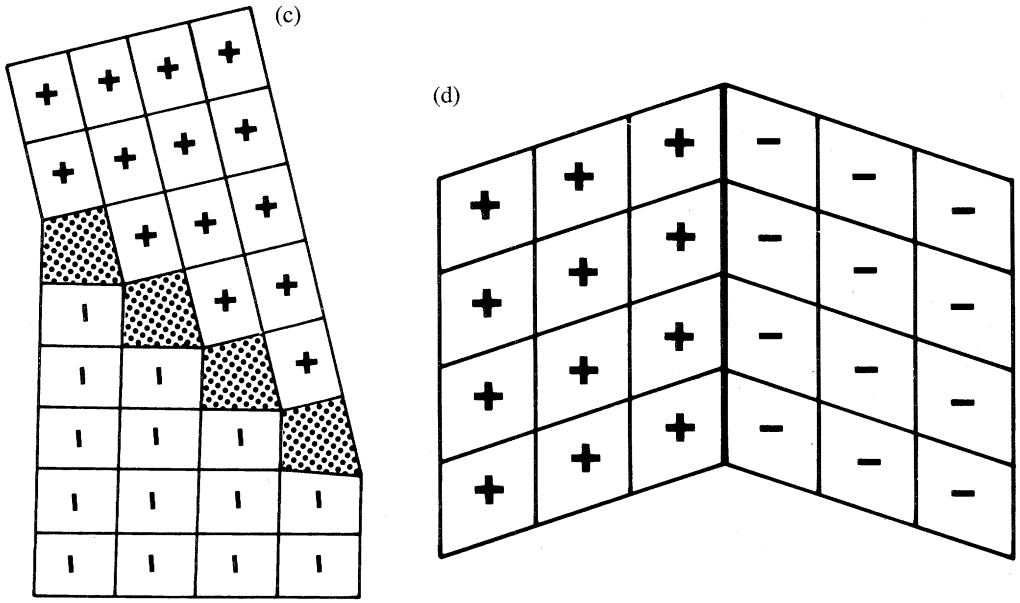

Figure 2. *Cont.* (*c*) Domain boundary for $e_{xx} = -e_{yy}$ type of strain, very idealized. Note the necessary distortion of the cells on the boundary. (*d*) Domain boundary for e_{xy} type of strain. Note the absence of any distortion around the boundary apart from the ordering strain.

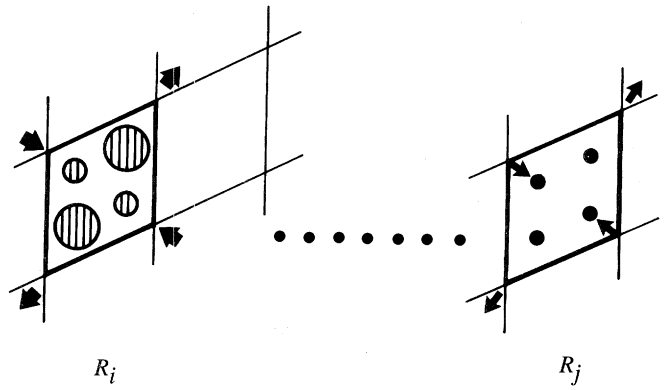

Figure 3. Origin of coupling mediated by strain (schematic). The ordering of two large and two small atoms distorts the cell shape at $\boldsymbol{R}_i$. The distortion results in forces (arrows) on neighbouring cells and is transmitted through the elastic medium (row of dots) to where it distorts the cell shape at $\boldsymbol{R}_j$, which in turn creates forces (arrows) tending to order atoms on the four sites in the cell (heavy dots).

$1/N$ to the total shear, and thus the factor $1/N$ stems from normalization. Although the Zener–Eshelby term is of order $1/N$, it gives a finite contribution to T_c and to the enthalpy per mole of the phase transition, when summed over all cells. It is also responsible for some of the phenomena to be mentioned below.

There is a second interesting feature of the interaction. In the ferroelastic case the interaction in the Fourier transform $J_{\boldsymbol{k}}$ has a singularity at $\boldsymbol{k} = 0$, in that the limit of $J_{\boldsymbol{k}}$ as $\boldsymbol{k} \to 0$ depends on the direction of $\boldsymbol{k}$. This is a simple reflection of the fact that the velocity of sound is anisotropic. It has observable consequences in the form

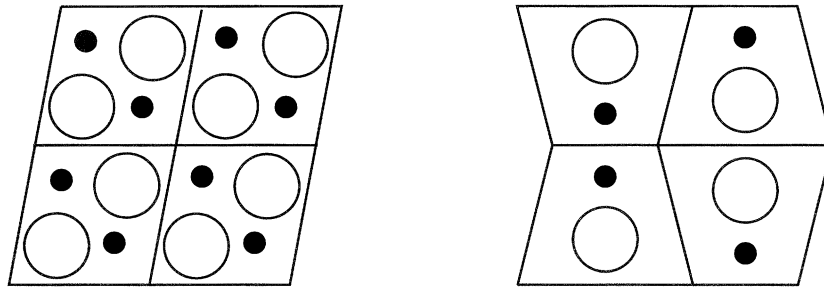

(a) (b)

Figure 4. (*a*) Ordering of two large and two small atoms in one cell creating a stress field of e_{xy} symmetry (ferroelastic). (*b*) The same with one large and two small atoms creating a stress field of trapezoidal symmetry on its surroundings, which results in antiferroelastic ordering.

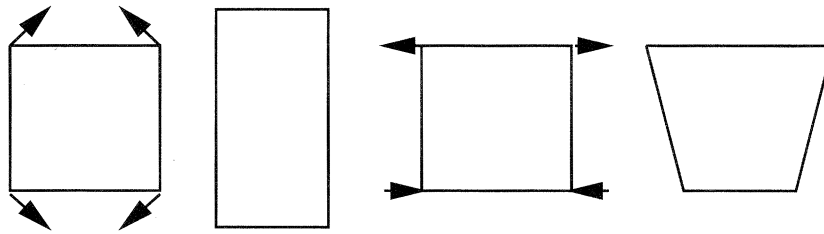

(a) (b)

Figure 5. Different symmetries of forces exerted by local ordering processes onto the neighbouring crystal sites: (*a*) stresses of e_{xx}–e_{yy} symmetry (ferroelastic) and (*b*) stresses of trapezoidal symmetry (cf. figure 4*b*).

of the fluctuations of the order parameter above T_c and the suppression of critical fluctuations (Bratkovsky *et al.* 1994*a*). The point of mathematical difficulties in the theory which we shall have to watch, arises from these two features, i.e. the volume term in (2.1) and the elastic anisotropy both contributing a singularity at $\boldsymbol{k} = 0$. Yet another point to take care of is the obvious existence of a *self-energy* which is due to initial deformation of the lattice due to local ordering process Q. It exists irrespective of other pseudospins in the system and, therefore, should be excluded from the *interaction* between Qs in different cells. Detailed analysis of all possible situations is given by Bratkovsky *et al.* (1995) and Tsatskis & Salje (1996).

Since the $J(\boldsymbol{R}_{ij})$ and the tweed texture are due to the strain generated by the structural transformation, the details of the atomic ordering geometry in each cell are of secondary importance: only the stresses caused on the neighbouring material matter. We shall, therefore, represent the local ordering process in a cell i by the scalar variable $Q(\boldsymbol{R}_i)$ and normalize it to ± 1 at $T = 0$, plus a resulting set of forces $\pm\boldsymbol{F}$ acting on the corners of neighbouring cells (figures 5*a*, *b*). $Q(\boldsymbol{R}_i)$ may be a discrete variable, as in a simple atomic ordering process, or it may be a continuous variable, such as the rotation angle of a (relatively rigid) unit, as previously defined. We can now write down the energy expression for the whole system in a general way as (Bratkovsky *et al.* 1994*c*, 1995)

$$E = \tfrac{1}{2}\boldsymbol{u}^{\mathrm{T}}\boldsymbol{\Phi}\boldsymbol{u} - \boldsymbol{u}^{\mathrm{T}}\boldsymbol{F}Q, \tag{2.3}$$

where $\boldsymbol{u}$ is now the column matrix of arbitrary atomic displacements, superscript 'T' denotes a transpose, and $\boldsymbol{\Phi}$ is the matrix of interatomic force constants as used in

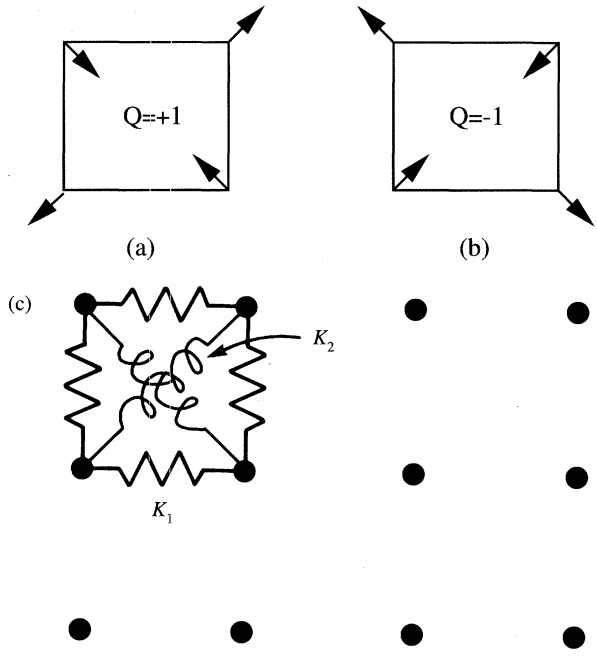

Figure 6. Schematic drawing of the ordered structural states corresponding (a) to the value of local ordering variable $Q = 1$ and (b) $Q = -1$. (c) Simple cubic structure (dots) connected by springs of strength K_1 and K_2 along the cube edges and diagonals (shown in one cell only).

lattice dynamics. Due to the fact that the energy (2.3) is a quadratic form of atomic coordinates, both atomic coordinates, $\boldsymbol{u}$, and local ordering variables (pseudospins), Q, can be decoupled by simple canonical transformation yielding an effective Hamiltonian:

$$E = NE_0 - \tfrac{1}{2}\sum_i \sum_{j(\neq i)} J(\boldsymbol{R}_{ij})Q(\boldsymbol{R}_i)Q(\boldsymbol{R}_j), \tag{2.4}$$

and the interaction (effective coupling) is given by

$$J(\boldsymbol{R}_{ij}) = [\boldsymbol{F}^{\mathrm{T}}\boldsymbol{\Phi}^{-1}\boldsymbol{F}]_{ij}, \tag{2.5}$$

where $\boldsymbol{\Phi}^{-1}$ is the lattice Green's function. It is quite clear from the form of the equations (2.4), (2.5) that all these expressions can be evaluated more easily in reciprocal space. There $\boldsymbol{\Phi}^{-1}$ can be found via the inverse dynamical matrix, diagonal in reciprocal space,

$$D^{\alpha\beta}_{\boldsymbol{k}} = \sum_{\boldsymbol{R}_{ij}} \Phi^{\alpha\beta}(\boldsymbol{R_{ij}}) \exp(-\mathrm{i}\boldsymbol{k}\cdot\boldsymbol{R}_{ij}), \tag{2.6}$$

the dimension of which is reduced dramatically due to Bloch's theorem compared to the original matrix of force constants. Then the energy (2.4) takes the form

$$E = E_0 - \tfrac{1}{2}\sum_{\boldsymbol{k}} J_{\boldsymbol{k}}Q_{\boldsymbol{k}}Q_{-\boldsymbol{k}}, \tag{2.7}$$

with the following expression for the interaction J:

$$J_{\boldsymbol{k}} = \begin{cases} \Omega_{\mathrm{c}} C_{\alpha\beta\gamma\delta} e^0_{\alpha\beta} e^0_{\gamma\delta} - P, & \text{for } \boldsymbol{k} = 0, \\ F^{\alpha}_{\boldsymbol{k}} (D^{\alpha\beta}_{\boldsymbol{k}})^{-1} F^{\beta}_{-\boldsymbol{k}}, & \text{for } \boldsymbol{k} \neq 0. \end{cases} \tag{2.8}$$

Here $P = 1/N \sum_{\boldsymbol{k}} F^{\alpha}_{\boldsymbol{k}} (D^{\alpha\beta}_{\boldsymbol{k}})^{-1} F^{\beta}_{-\boldsymbol{k}}$ is the self-energy, the $\boldsymbol{k} = 0$ term corresponds to the infinite-range Zener interaction between Qs in real space:

$$J_{\mathrm{Z}} \equiv Z/N = (1/N)(\Omega_{\mathrm{c}} C_{\alpha\beta\gamma\delta} e^0_{\alpha\beta} e^0_{\gamma\delta} - P). \tag{2.9}$$

For actual simulations we have used a local order parameter Q_i having only the values of ± 1 (a pseudospin (figures 6*a*, *b*)) in a simple cubic lattice where first and second neighbours were coupled by elastic springs to represent a deformable solid (figure 6*c*). Due to its simplicity all quantities of interest can be calculated easily, many of those, like the dynamical matrix, etc. in closed form. Simulations have been performed with a combined Monte Carlo–molecular dynamics algorithm to, first, prepare a Q-configuration and, second, relax atomic positions subject to forces exerted by the local ordering processes Q. We have updated the pseudospin configuration $\{Q\}$ following Glauber spin dynamics attached to a heat bath at the given temperature. Once the spin configuration has been chosen, we have solved the Newtonian equations of motion with a fictitious friction force to find out new equilibrium ionic positions. The procedure is exactly equivalent to a Monte Carlo algorithm applied to the combined ordering plus relaxation energy due to the assumption of harmonic springs. This model has given remarkably 'life-like' images of tweed in computer simulations (Bratkovsky *et al.* 1994*b*, *c*) as we shall describe later.

In the ferroelastic case the ridges of $J_{\boldsymbol{k}}$ coincide with directions in which material may have infinitely long coherent domain walls separating domains with different spontaneous deformation e. The conditions for coherent macroscopic domain walls between regions of strain $e^{(1)}$ and $e^{(2)}$ are (Sapriel 1975)

$$\det(e^{(1)}_{\alpha\beta} - e^{(2)}_{\alpha\beta}) = 0, \quad \mathrm{tr}(e^{(1)}_{\alpha\beta} - e^{(2)}_{\alpha\beta}) = 0, \tag{2.10}$$

where det and tr denote the determinant and the trace of a matrix, respectively. We only consider cases where $e^{(2)} = -e^{(1)}$, and it is easy to check that for the typical case of the xx–yy type of strain (i.e. $e_{xx} = -e_{yy} \neq 0$), as well as for the xy shear, the Sapriel conditions (2.10) are satisfied. Incidentally, there is a clear non-additivity of different eigenstrains. For instance, e_{xy}, e_{yz} and e_{xz} all satisfy the Sapriel conditions (2.10), but their sum, $e_{xy} + e_{yz} + e_{xz}$, which corresponds to cubic to rhombohedral transformation, does not.

When the conditions (2.10) are satisfied, the domain walls can have two orientations with normals $\boldsymbol{n}_1$ and $\boldsymbol{n}_2$ that are at right angles: hence the tweed texture. This has nothing to do with symmetry and applies, for instance, to triclinic feldspars. For the xy shear these are the [100] and [010] planes, and for the xx–yy shear they are the $[1, \pm 1, 0]$ planes.

Returning briefly to real crystals and their phase transitions we should note that their atomic structure cannot always be mapped directly onto our simplified model. But we believe that our model contains the physics displayed by them. For instance, in KCN, the CN^- ion can point in several possible directions, leading to a multicomponent order parameter and several types of domains with different strains $e^{(s)}$ (Michel & Theuns 1989); but the existence or otherwise of coherent boundaries depends again on Sapriel's conditions (2.10).

PHILOSOPHICAL TRANSACTIONS OF THE ROYAL SOCIETY A MATHEMATICAL, PHYSICAL & ENGINEERING SCIENCES

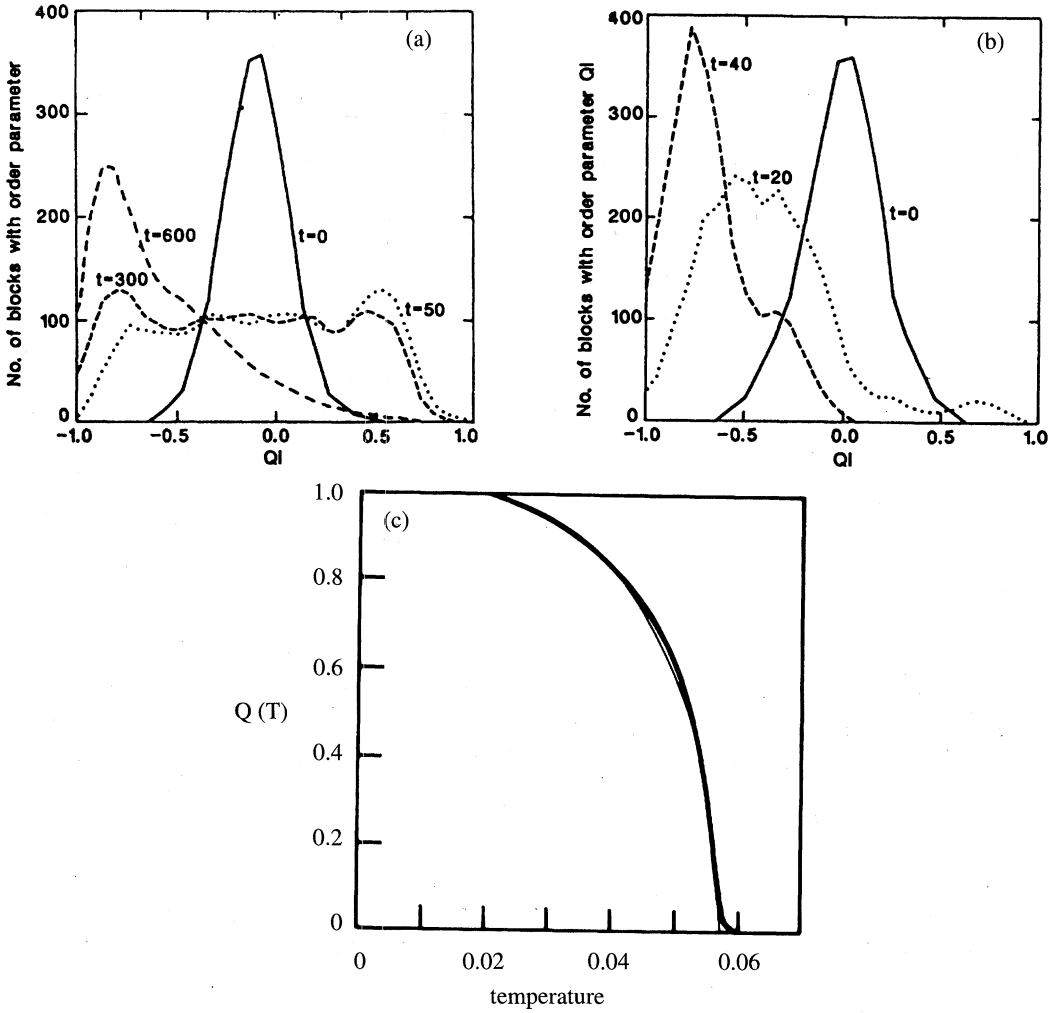

Figure 7. Profiles of the number of $3 \times 3 \times 3$ sub-blocks with a certain value of Q_i in our computer model after quenching from far above T_c to around $0.9T_c$. Different profiles correspond to different times after the quench in units of Monte Carlo steps per ordering variable. (*a*) Direct nearest neighbour coupling between the ordering variables Q_i (*b*) strain coupling of $e_{xy}+e_{yz}+e_{xz}$ symmetry. (*c*) Temperature evolution of the order parameter model with strain coupling of $e_{xy}+e_{yz}+e_{xz}$ symmetry which does not allow for coherent domain walls in a computer simulated (bold line) and in mean field theory (thin line).

3. Effect of local strain on ordering kinetics and textures

As a result of the long ranged behaviour of the coupling $J(\boldsymbol{R})$ (2.1) we can expect the mean field Bragg–Williams theory to be exact (Vaks *et al.* 1966). It is important to note that the angularly dependent term in equation (2.1) has zero angular average and does *not* contribute to the mean field transition temperature. However, due to the anisotropy of this term it determines the short-range order and results in tweed pattern, as we discuss below. The critical temperature of transition (in the absence of short range interactions) would be determined by only the Zener–Eshelby term

J_Z, and in the mean field approximation

$$k_B T_c^{\text{strain}} = N J_Z = \Omega_c C_{\alpha\beta\gamma\delta} e^0_{\alpha\beta} e^0_{\gamma\delta} - P. \tag{3.1}$$

The behaviour of the order parameter has been analysed in simulations for our strain coupled model, described previously, and gives *bona fide* phase transition (Bratkovsky *et al.* 1994*c*; Marais *et al.* 1994). In this case the simulation has been done for a three-dimensional $16 \times 16 \times 16$ lattice with a set of forces $\boldsymbol{F}$ producing a stress of the type $xy + yz + xz$ (which prohibits the existence of coherent domain walls). The temperature dependence of the order parameter, defined as

$$Q = \frac{1}{N} \sum_i Q(\boldsymbol{R}_i) \tag{3.2}$$

for ferroelastic transitions, follows the behaviour of mean field theory very well, as seen in figure 7*c*.

The kinetics of ordering in our strain interaction model differ from those predicted by 'nucleation and growth' theories and observed in nearest-neighbour Ising models. The long-range elastic interactions couple all the local ordering variables to one another, resulting in a uniform ordering of the system. In figure 7 the distribution of a coarse-grained order parameter Q is shown as the system orders. The coarse grained Q_i is the average of $Q(\boldsymbol{R}_i)$ over the block of $3 \times 3 \times 3$ cells centred on cell i. Initially Q_i is distributed around zero with a statistical width of $1/\sqrt{27}$ as expected from the $3 \times 3 \times 3$ coarse graining. Figure 7*a* shows the behaviour of a conventional Ising system with nearest-neighbour coupling. At $t = 50$ the system has evolved a broad distribution showing substantial clusters forming with Q_i near to the equilibrium values $Q_i = \pm Q_{\text{eq}} \approx \pm 0.8$ with boundaries between these regions accounting for the distribution in between the two values $\pm Q_{\text{eq}}$. Only after a very much longer time do the clusters with negative Q_i (in this particular simulation) grow at the expense of the positive clusters to give the final ordered state, not yet fully reached at $t = 600$.

This is in stark contrast with the behaviour of the strain coupled system shown in figure 7*b*. Throughout the ordering process the system remains essentially uniform with the distribution retaining the form of a narrow peak. As the ordering evolves, this peak moves relatively uniformly to its value at Q_{eq} (negative in this case). The reason is that every cell 'knows what every other cell is doing' in the whole sample because of the long-range nature of the interaction. There are no signs of the local 'nucleation and growth' processes observed in figure 7*a*.

Having shown that the sample orders uniformly, one can develop a theory of (dis)ordering kinetics which leads to relatively simple rate laws describing the order parameter growth. The kinetic theory of second-order phase transitions is discussed in detail by, for example, Landau & Khalatnikov (1954), Patashinskii & Pokrovskii (1979), Khachaturyan (1983), Dattagupta *et al.* (1991*a*, *b*).

The uniform ordering process which we observe in our model can, to a good approximation, be described within the scope of the time-dependent Landau–Ginzburg equation

$$\frac{\partial Q}{\partial t} = -\hat{\nu} \frac{\delta G_L}{\delta Q}, \tag{3.3}$$

where $G_L = G_L[Q]$ is the appropriate free-energy Landau functional, $\hat{\nu} = -\nu_c \nabla^2 + \nu_n$, ν_n and ν_c are the kinetic coefficients for non-conserved and conserved order parameters, respectively (Landau & Lifschitz 1986; Patashinskii & Pokrovskii 1979).

PHILOSOPHICAL TRANSACTIONS OF THE ROYAL SOCIETY A MATHEMATICAL, PHYSICAL & ENGINEERING SCIENCES

In this theory an account can also be made for strain interaction (Dattagupta *et al.* 1991; Salje 1993*a*, *b*; Khachaturyan 1983; Semenovskaya & Khachaturyan 1991*a*, *b*; Chen *et al.* 1992). In case of a partially conserved order parameter, a complex pattern is expected as the outcome of kinetic processes (Salje 1993*b*; Tsatskis *et al.* 1994).

Usually the Landau functional is used which is known to be correct close to the equilibrium configuration. Such rate laws have been extensively tested experimentally and found to describe the observed (dis)ordering behaviour correctly (see, for example, Salje *et al.* 1993). In some situations, however, the system is far from equilibrium, and the applicability of the Landau functional derived close to equilibrium becomes questionable (Marais *et al.* 1991*b*, *c*; Marais & Salje 1991; Salje 1993*a*, *b*).

The major effect on kinetics of ferroelastically coupled systems which allows the existence of coherent domain walls (as for xx–yy and xy shears) is that it goes into a metastable texture during ordering and never (or very slowly) orders. To illustrate the point we give here the results of our simulations of the system with the strain coupling of ferroelastic symmetry xx–yy (figure 8). We can see that immediately after the quench to below the critical temperature the system arranges itself into a tweed pattern consisting of multiple domain walls mainly aligned with the [1,±1,0] soft directions (figures 8*a*, *b*). This tweed microstructure gives way to larger domains in figures 8*c*–*f* leading to large areas where only parallel domain boundaries occur. This finishes the first (fast) stage of the coarsening and further kinetics slows down as the number of domain wall junctions reduces. We can see how one group of domains disappears to leave the more regular stripe pattern. This process is stepwise and involves *needle*-domain formation (figures 8*c*–*f*) often seen in ferroelastics (Bratkovsky *et al.* 1994*c*). Already in figure 8*c* we see that some domains in the right part of the simulation sample have developed bumps which bend towards each other and eventually merge. The domains of opposite sign take, consequently, the needle-shaped form which is clearly seen in figure 8*d*. They cut free from the stripe and pull back to complete the formation of a new stripe in figure 8*c*; and so on in a self-similar way.

The physical origin of needle domains is as follows (Bratkovsky *et al.* 1994*c*). The right-angle domain wall causes a lattice misfit and related elastic distortion which the system tries to accommodate. If we imaging cutting out domains from perfectly transformed crystals and fitting them together, there would be thin wedge-shaped gaps or overlaps of angle $2e_0$ at the joins, where e_0 is the spontaneous strain of the transformation. Thus fitting the domains together maintaining lattice coherence requires local stress fields which can be visualized conveniently as if they were produced by a set of *fictitious* dislocations with Burgers vectors proportional to e_0 (Miltat & Kléman 1973). The total force between the corners is *attractive* and can be easily evaluated:

$$F = -\frac{\mu e_0^2}{\pi(1-\sigma)} a \ln(L/a), \tag{3.4}$$

where μ and σ are the shear modulus and Poisson ratio, respectively, and L stands for the usual upper cut-off distance. The typical value of the prefactor in equation (3.4) is of the order of a few kbar.

Finally, the kinetics of the coarsening process has been found in the simulations to give a T–T–T (time–temperature–transformation) diagram similar to those typically observed (Parlinski *et al.* 1993*a*, *b*).

Other examples are those for a 'non-Sapriel' ferroelastic $2zz$–xx–yy (figure 9*a*, *b*) and an antiferroelastic strain (figure 9*c*, *d*). The domain walls do appear in these cases as well, but they have very irregular shape (Heine *et al.* 1994; Marais *et al.*

PHILOSOPHICAL TRANSACTIONS OF THE ROYAL SOCIETY A MATHEMATICAL, PHYSICAL & ENGINEERING SCIENCES

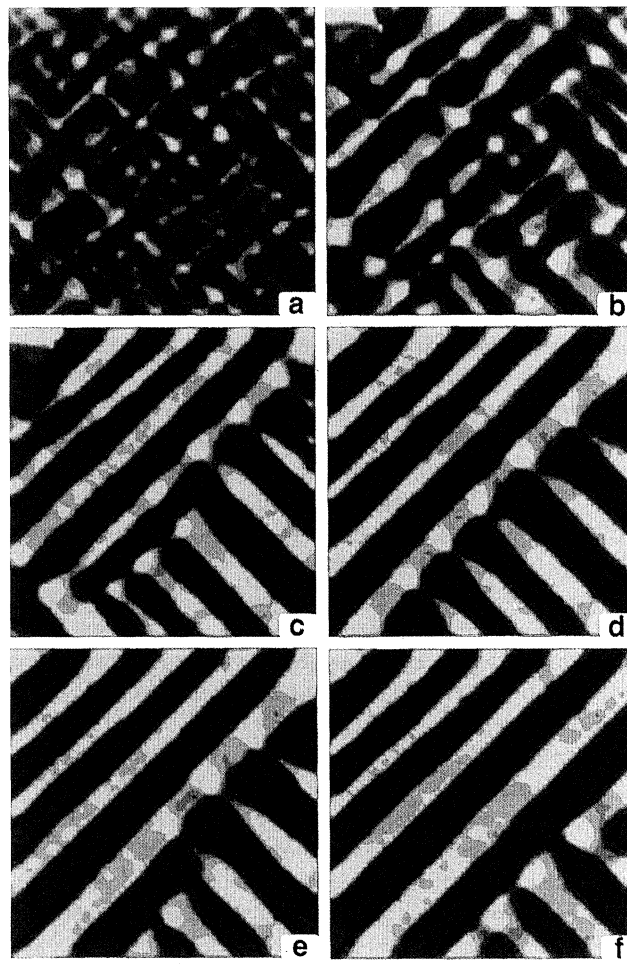

Figure 8. The maps of strain order parameter obtained during annealing at temperature $T_a = 0.43T_c$ after quenching from $T = 2T_c$. Those from (a)–(f) correspond to annealing time $t = 10$, 50, 200, 1000, 2000 and 4000 Monte Carlo steps per site. Note the immediate appearance of tweed in (a) due to the pre-existence of embryos at $2T_c$, the sharpening up of microdomain walls in (b), the coarsening in (b), (c), and the formation of needle domains in (d)–(f).

1994). In the former case this is due to violation of the Sapriel conditions (2.10) for the existence of straight domain walls. In the 'non-Sapriel' case the simulated systems with free boundaries have quickly ordered into a single domain below T_c (figure 9*a*). However, with *clamped* boundaries this is prohibited and the system always forms a developed domain pattern (figure 9*b*) to relieve the strain energy as observed experimentally. The antiferroelastic case is different because there the existence of straight domain walls is not prohibited, but their low energy allows easy bending. This follows from equation (2.2) and is connected with the fact that in the antiferroelastic case the interaction is more short ranged ($\propto 1/R^5$) compared to the ferroelastic case.

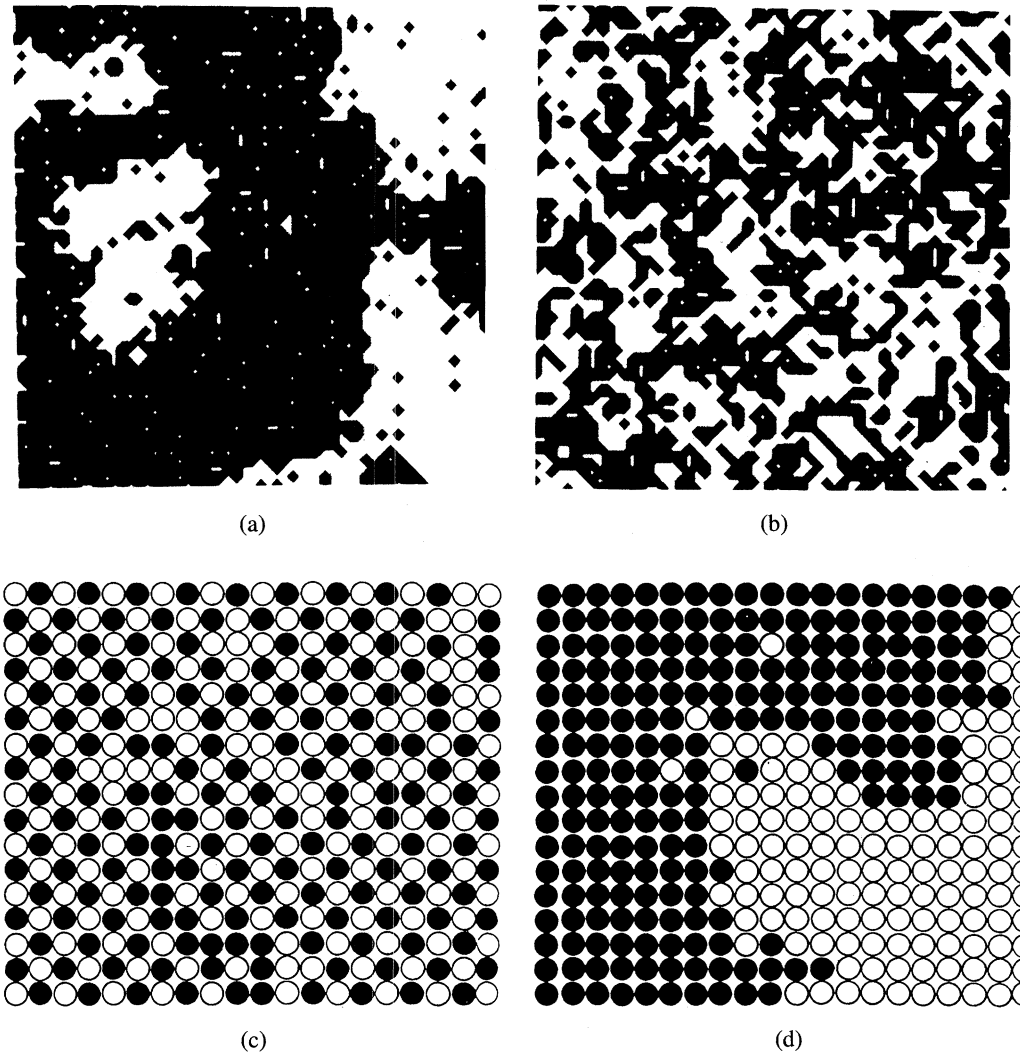

Figure 9. (*a*) The maps of the spin order parameter obtained during annealing of clamped samples at temperature T_a after quenching from $4T_c$. (*a*) $T_a = 0.8T_c$ clamping of x-, y- and z-faces. (*b*) $T_a = 0.9T_c$, clamping of x- and y-faces. Note a few coarse irregular domains in (*a*) where all faces were clamped. (*c*) Antiferroelastic domain wall with strain deformation as shown schematically in figure 5*b*. (*d*) the same domain wall can be made more visible if ordering variables are multiplied by a phase factor $\exp(i\pi(x+y))$.

4. The origin of tweed texture

We have discussed in previous sections the general features of strain-mediated interactions and noted that the long range and anisotropy of this interaction always results in some form of texturing (tweed) of material during ordering when the Sapriel conditions are satisfied. It is important to discuss where the tweed texture really comes from. Prior to our work, it appears to have been thought that the *origin* of tweed is a kinetic effect occurring only when the material has reached a temperature below T_c in a quench experiment (Khachaturyan 1983; Wen *et al.* 1981; Tanner *et al.* 1982; Robertson *et al.* 1983; Zhu *et al.* 1991; Chen *et al.* 1992).

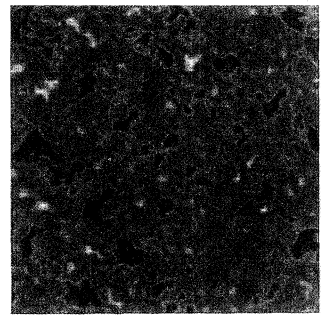

Figure 10. The map of the strain order parameter at temperature $1.3T_c$ showing the embryonic fluctuations for a system with e_{xx}–e_{yy} type of coupling and boundaries of the type in figure 2*c*.

However our work has shown, both analytically and by computer simulations, that the tweed-like short-range order or 'tweed embryos' exist as thermodynamic fluctuations at temperatures well above $T_c = T_c^{\text{strain}}$, even $2T_c$ and higher (figure 10). On a long time scale they do of course fluctuate, but they do so very slowly. In a quench, they are simply frozen in, and then sharpen up and coarsen as already described in connection with figure 8. Our picture has an important practical consequence: the scale of the texture can be influenced by the temperature at which the material is annealed above T_c before quench, as has been done with YBCO. We note that embryonic fluctuations have also been invoked to explain pretransitional phenomena in martensitic (first-order) phase transitions where the order parameter is strongly coupled to strain (Seto *et al.* 1990).

In order to gain more insight into the origin of textures (especially tweed) in ferroelastic materials we have undertaken extensive computer simulations of our simple model introduced in § 2 *obeying* the Sapriel conditions (2.10) for the existence of coherent domain walls. We observed the evolution of the model subject to Glauber (i.e. non-conserved) kinetics for the local ordering processes Q with atomic positions adjusted to the instantaneous configuration of (pseudospins) Q. An important aspect of our studies is that we do not rely on any particular form of the Landau free energy or approximation for the stress field. The system is driven towards equilibrium by elastic forces and by the principle of detailed balance for the thermodynamic behaviour, and we simply observe how it evolves. Although the model to which we apply the laws of physics is a simplified one, it picks out and treats exactly the strain effects.

We have considered the model with e_{xx}–e_{yy} type of spontaneous strain relevant for the orthorhombic-to-tetragonal (O–T) phase transition in $YBa_2Cu_3O_{7-\delta}$. The structural O–T phase transition occurs at temperature $T_c \approx 1000$ K (Jorgensen *et al.* 1987). The approximation of the model is that we ignore all other interactions, e.g. screened Coulomb interactions in our studies of oxygen (dis)ordering in YBCO (Bratkovsky *et al.* 1994*b*; Parlinski *et al.* 1993*a*, *b*). We note, however, a variety of short-period superstructures due to oxygen ordering observed in oxygen-deficient YBCO (Reyes-Gasga *et al.* 1989). These superstructures were successfully explained in terms of a short-range interaction model (Poulsen *et al.* 1991; Adelman *et al.* 1992, and references therein), and the inclusion of Coulomb effects has been shown to be important (Aligia & Garces 1994; Aligia 1992). Moreover, the short-range interactions determine the temperature of the orthorhombic-to-tetragonal phase transition

in YBCO, as is seen from the following simple calculation. On the other hand, that model obviously cannot explain the tweed and stripe textures which are the result of long-range elastic interactions.

It is easy to estimate the critical temperature of the O–T ferroelastic phase transition in YBCO with the use of equation (3.1) (Brown 1995). Using the lattice parameters of the orthorhombic phase $a = 3.820$ Å, $b = 3.885$ Å, $c = 11.681$ Å (Schmahl *et al.* 1989; David *et al.* 1987) and $a_t = 3.854$ Å for the tetragonal phase of YBCO (Schmahl *et al.* 1989) we can estimate the spontaneous strains of the O–T transformation $e_{11} = (a-a_t)/a_t = -0.0088$ and $e_{22} = (b-a_t)/a_t = +0.0080$. We can approximate it rather accurately by a spontaneous strain $e_0 = (e_{22}+|e_{11}|)/2 = 0.0084$ of pure xx–yy symmetry, and then write down the corresponding mean field expression for the critical temperature as $T_c^{\mathrm{strain}} = 2\Omega_c(C_{11} - C_{12})e_0^2 - P \approx 260$ K. In this estimate we have used the experimental values for elastic constants $C_{11} = 3.73 \times 10^{11}$ N m^{-2} and $C_{12} = 2.08 \times 10^{11}$ N m^{-2} (Baetzold 1988). The estimated value $T_c^{\mathrm{strain}} = 260$ K and we see that the long-ranged elastic effects account for under 30% of the actual O–T phase transition in YBCO.

First we discuss the results of our simulations at temperatures well above T_c with strain coupling of the xx–yy symmetry (Bratkovsky *et al.* 1994*b*). At $T \sim 2T_c$ we found well-defined embryos of the tweed texture as shown in figure 10. As well as being tweed-like in shape, the local strain in them attains an appreciable fraction (*ca.* 50%) of the maximum spontaneous strain at low temperature. The embryos existing above T_c before quenching become the metastable tweed texture after quenching.

There are even well-defined embryos at $4T_c$ and higher temperatures, although less intense of course. This is relevant to YBCO because $4T_c$ in our model translated into $4T_c^{\mathrm{strain}}$ there, which is approximately the actual T_c of YBCO. Thus we certainly expect our story of the origin of the tweed texture on cooling to apply to YBCO, although the high temperature relative to T_c^{strain} may make embryos difficult to verify experimentally above T_c. From the quantitative theory below, we can estimate that the local strain attained in the embryos is of order 35% of the maximum spontaneous strain. This is enough to seed the tweed texture on quenching.

The disorder in our model is dominated by strain-induced microdomains with boundaries approximately parallel to $[1,\pm1,0]$. It is interesting to compare the fluctuations of the order parameter measured in simulations:

$$S_{\boldsymbol{k}} = \langle Q_{\boldsymbol{k}} Q_{-\boldsymbol{k}} \rangle, \tag{4.1}$$

where

$$Q_{\boldsymbol{k}} = \frac{1}{N} \sum_i Q(\boldsymbol{R}_i) \exp(\mathrm{i}\boldsymbol{k} \cdot \boldsymbol{R}_i), \tag{4.2}$$

with predictions of a theory of classical uncorrelated fluctuations which gives (Landau & Lifschitz 1986)

$$S_{\boldsymbol{k}} = \frac{k_B T}{k_B T - J_{\boldsymbol{k}}}. \tag{4.3}$$

The behaviour can best be understood by approximating $J_{\boldsymbol{k}}$ for small k as

$$J_{\boldsymbol{k}} = d(\boldsymbol{n}) - g(\boldsymbol{n})k^2, \tag{4.4}$$

where $\boldsymbol{n} = \boldsymbol{k}/k$ and the functions d and g depend only on the symmetry of coupling, and $d(\boldsymbol{n})$ reaches its maximum value only along the symmetry directions of the

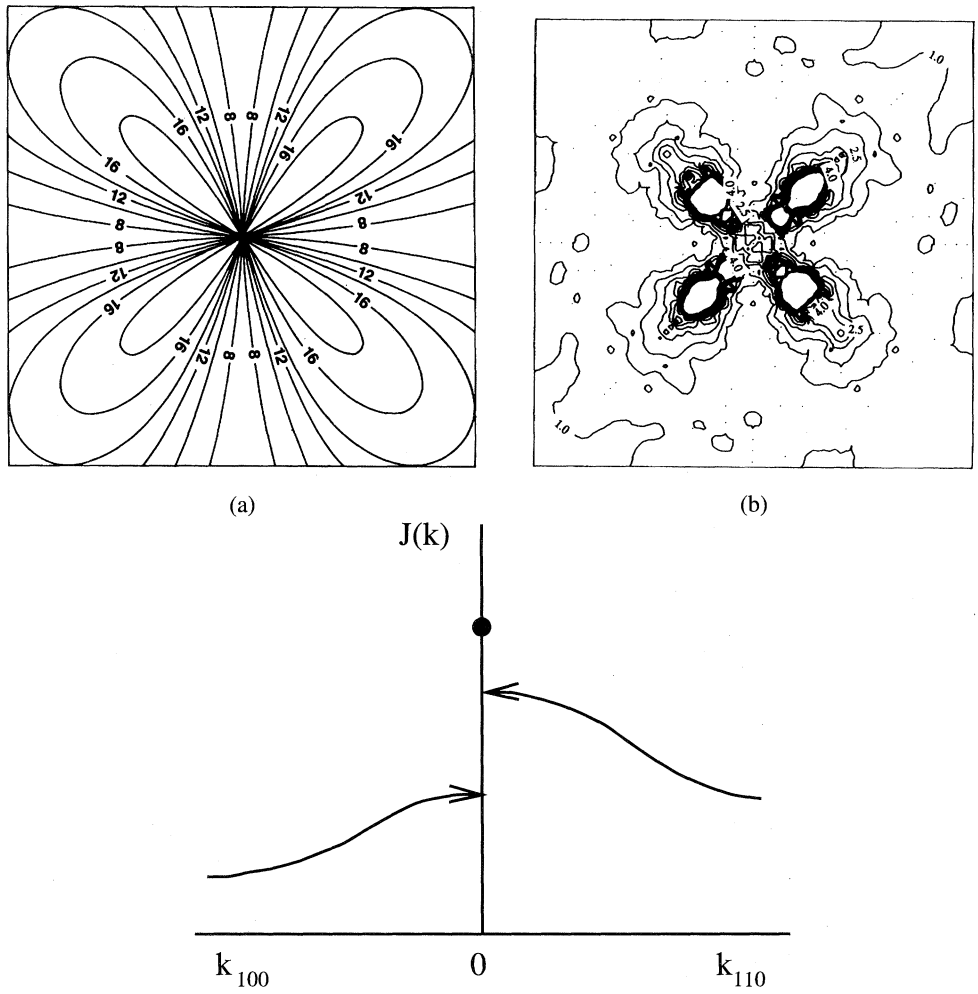

Figure 11. (*a*) The coupling $J_{\boldsymbol{k}}$ for e_{xx}–e_{yy} type of strain; (*b*) the structure factor $S_{\boldsymbol{k}}$ from the simulations above T_{c}; (*c*) the most general form of the interaction $J_{\boldsymbol{k}}$ in reciprocal space. The value $J_{\boldsymbol{k}} = 0$ is larger or equal to the limit $\boldsymbol{k} \to 0$ in any direction.

lattice, which are defined as the 'soft' directions where the fluctuations are enhanced (Bratkovsky *et al.* 1993*a*).

Comparison of $J_{\boldsymbol{k}}$ calculated from (2.8) and the measured $S_{\boldsymbol{k}}$ in the model at $T = 1.3T_{\mathrm{c}}$, displayed in figure 11, shows almost the same butterfly-like pattern. For the sake of completeness, we show in figure 11*c* the most general form of the interaction $J_{\boldsymbol{k}}$ in reciprocal space, which illustrates the non-analytic behaviour of the interaction at small wavevectors.

The fluctuations along hard directions are suppressed and 'arms' of large $S_{\boldsymbol{k}}$ are extended along [1,±1,0] directions. The difference between the two patterns is limited to the region at $ka_0 \sim 0.15$ where we observe a strong saturation effect. There the measured $S_{\boldsymbol{k}}$ has its minimum instead of reaching a flat maximum prescribed by the simple Ornstein–Zernike formula (4.3). This is related to the fact that already at $T \sim 2T_{\mathrm{c}}$ the system shows some tendency to regularize the spatial fluctuations into roughly equally spaced parallel domains. Thus (coming down in T) the fluctuations

already deviate from the classical form (4.3) at $T \sim 2T_c$, and this is a saturation effect from the fact that the local order parameter in our model cannot exceed the value at $T = 0$. In a Landau development of the free energy the effect would come from Q^4 and higher-order terms in the entropy. In that qualitative sense the deviation of the fluctuations from classical form has a similar origin to that in critical fluctuations. However the usual long wavelength and scaling behaviour of critical fluctuations do not apply to our tweed embryos because of the unusual form of (4.4).

It is worth noting that the observed fluctuations stem from the behaviour (4.4) of the coupling $J_{\boldsymbol{k}}$, or, more precisely, from the term $d(\boldsymbol{n})$ with its strongly non-analytic behaviour for small $\boldsymbol{k}$. This term prevents domain walls from curving as they do when $d(\boldsymbol{n}) = 0$, as in antiferroelastic systems. Our simulations show, indeed, that antiferroelastic systems show behaviour intermediate between that of the ferroelastic case and a nearest-neighbour Ising model insofar as domain walls easily nucleate and have arbitrary shape.

5. 'Non-thermodynamic' behaviour on rapid heating

There is current interest in a wide range of phenomena where a non-equilibrium system does not follow the obvious direct path towards equilibrium. They include structural transformations under sudden heating or sudden release of pressure. A system in this situation is put into a highly non-equilibrium state and can explore unusual paths towards its equilibrium state. Examples are the amorphisation of crystalline silica under pressure (Hemley *et al.* 1988; McNeil & Grimsditch 1992; Doukhan 1994) or release of pressure (Tsuji *et al.* 1993), transient phases in a–Si on rapid heating (Masaki *et al.* 1995), possibility of domains 'switching' in a ferroelectric subjected to a high-intensity optical pulse of a period much shorter than the typical phonon period (Fahy & Merlin 1994), and others.

We thought it would be important to see whether our model, which is simple enough to allow complete understanding of its behaviour, can reproduce the effect. We have, therefore, performed a series of computer experiments where we started from the completely ordered state, $Q = 1$. Then the pseudospins in the model were set free at temperature $T \approx 0.5T_c$. According to a standard picture of thermodynamic behaviour, the system would have kept its ordered state with a high degree of order, only a few 'wrong' spins were expected to appear during equilibration of the system. But the actual behaviour has been completely different from the prescribed picture: first, spin flips occur randomly across the lattice (figure 12*a*). Second, those that are roughly in $\pm(1, \pm 1, 0)$ directions from one another set up local strain fields which develop into microdomains along the soft directions in the crystal (figure 12*b*). Thus, the system instead of remaining slightly disordered at low temperature finds its way towards a tweed pattern. Macroscopically this specimen would look completely disordered though inside each domain the degree of order is almost perfect, with all the disorder concentrating inside the domain walls. Trying to find the relation of the model behaviour with the real world we can speculate as follows. The critical temperature of the phase transition is $T_c \sim Ce_0^2$, where C is a typical elastic constant of the material. It is reasonable to expect that under pressure p the stiffness increases, $C(p) > C(0)$ and T_c goes up, then the decompression would correspond to a sudden increase of T/T_c, as in our computer model.

We believe that this evolution of the system under conditions of sudden heating towards the tweed pattern is a useful paradigm of a 'non-thermodynamic' behaviour,

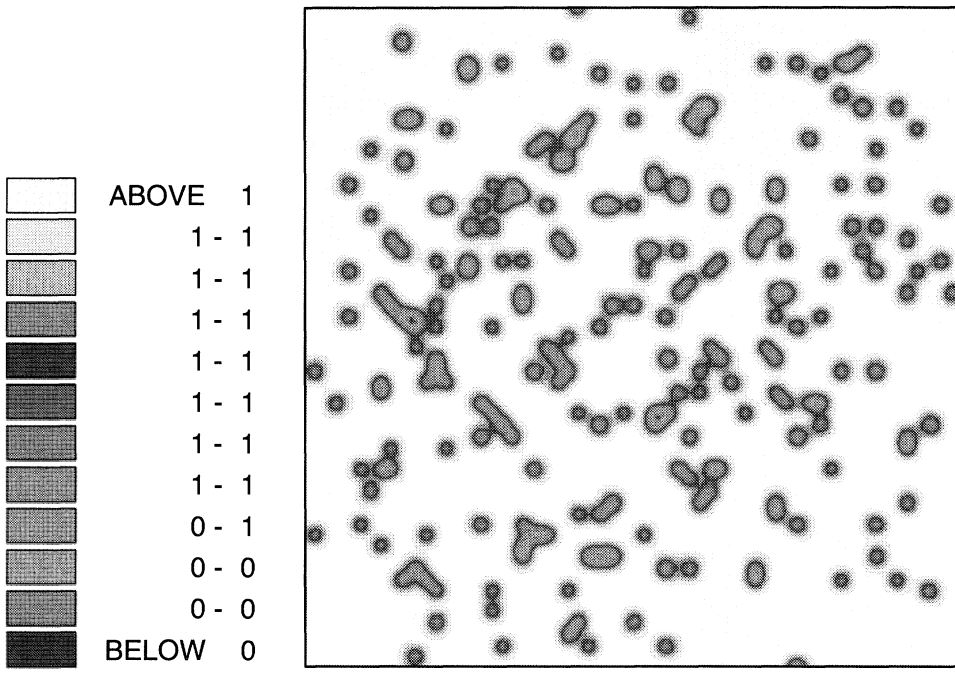

Figure 12. Sudden heating: model system which has initially been set in state with all $Q_i = 1$ and then subjected to instant heating to $0.4T_c$. (a) After $t = 2$ Monte Carlo steps a few spins have flipped in rather random manner.

when a system during (dis)ordering gets trapped in a 'wrong' free energy minimum and never gets out from there.

6. Conclusions

We have discussed a variety of phenomena in phase transitions related to strain. Strain accompanies almost any kinetic ordering process in the bulk or surface and leads to elastically mediated interaction. The elastic interaction $J(\boldsymbol{R}_{ij})$ falls off slowly, usually as the inverse cube of the distance R, and also contains an important term of infinite range, the so-called Zener–Eshelby interaction. Although the elastic interactions have long been studied in the case of point defects in solids, in ferroelastics it is seen in its 'pure' form and leads to a *bona fide* phase transition.

The general form of interaction J_{ij} between local ordering processes in ferroelastics is completely defined by the symmetry of the order parameter strain coupling. We have shown that the coupling with the symmetry of the macroscopic strain leads to ferroelasticity, otherwise to antiferroelasticity. Generally, in the ferroelastic case the interaction $J(R) \propto 1/R^3$, in the antiferroelastic case $J(R) \propto 1/R^5$. These laws are qualitatively different in the sense that the ferroelastic interaction has long (infinite) range, whereas antiferroelastic is short ranged, close to systems with nearest-neighbour interaction. It makes all the difference in their properties with respect to their thermodynamic and kinetic behaviour.

There is a drastic difference in the kinetic behaviour and textures in ferroelastics with twin boundaries (Sapriel case) and otherwise (non-Sapriel case). In a Sapriel fer-

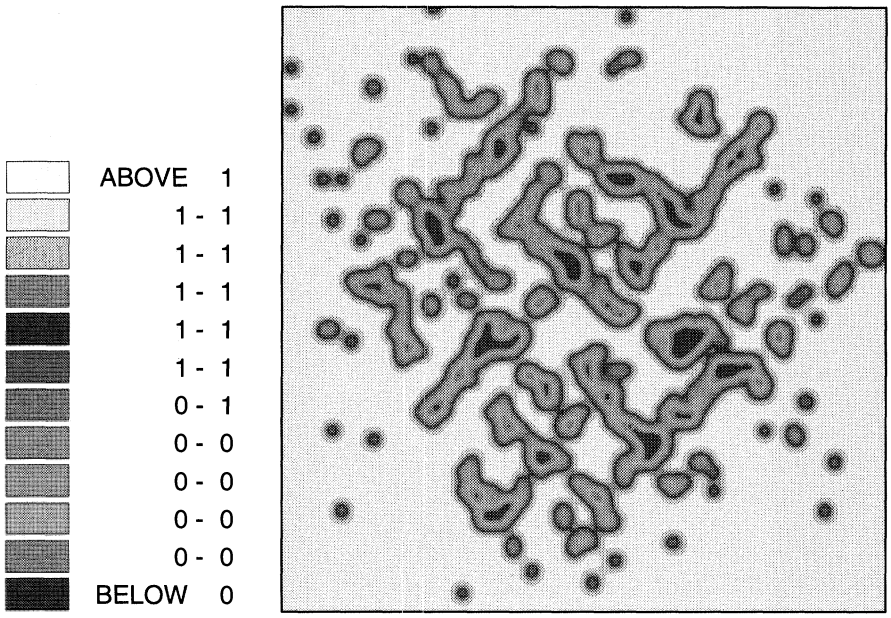

Figure 12. *Cont.* (*b*) After $t = 50$ Monte Carlo steps the long range elastic interaction between ordering variables resulted in tweed.

roelastic system there is always a tendency to produce a dense mass of microdomains and quickly develop a cross-hatched 'tweed' pattern of domain walls running in two soft directions inside a material. Although tweed is a state unfavourable thermodynamically compared to the well-ordered system, the systems tend to get trapped in this state and relatively slowly evolve into a 'stripe' phase with fewer domain boundaries.

Non-Sapriel ferroelastics quickly order into uniform mesoscopic domains because all the domain boundaries cost a lot of elastic energy: there is no 'nucleation and growth'. This behaviour implies the applicability of standard rate laws for second-order phase transitions (Landau & Khalatnikov 1954; Patashinskii & Pokrovskii 1979) to ferroelastic systems (Salje 1993*a*, *b*).

In ferroelastics with coherent twin boundaries (dis)ordering always involves some kind of domain pattern, in many cases tweed-like. The stage of tweed pattern seems to be unavoidable in cases studied analytically and on computer (Bratkovsky *et al.* 1994*c*) and in experiment (Salje 1993*a*; Khachaturyan 1983). The most dramatic example of texturing is that of a rapid heating of an ordered system to some temperature well below the critical temperature T_c. In this case an initial completely ordered state quickly evolves into a tweed state due to anisotropic elastic forces acting between local ordering processes operating over long distances. A lot of disorder appearing in this case is apparently against simple expectation of the disorder corresponding to a given final temperature. The system develops a tweed pattern and stays in this metastable state for a long time. The latter observation should be relevant for processes of unusual kinetic behaviour of systems subjected to a shock heating (Fahy & Merlin 1994) which it would be interesting to investigate experimentally.

References

Adelman, D., Burmester, C. P., Wille, L. T., Sterne, P. A. & Gronsky, R. 1992 Long-range interactions, long-range order and devil's staircase in $YBa_2Cu_3O_x$. *J. Phys.* C **4**, L585.

Aligia, A. A. 1992 Atomic structure of $YBa_2Cu_3O_{6+x}$ determined by Coulomb repulsion. *Europhys. Lett.* **18**, 181.

Aligia, A. A. & Garces, J. 1994 Charge-transfer and oxygen ordering in $YBa_2Cu_3O_{6+x}$. *Phys. Rev.* B **49**, 524.

Benkert, C., Heine, V. & Simmons, E. H. 1987 The incommensurate phase-transition of biphenyl *J. Phys.* C **20**, 3337.

Bratkovsky, A. M., Marais, S. C., Heine, V. & Salje, E. K. H. 1994*a* The theory of fluctuations and texture embryos in structural phase-transitions mediated by strain. *J. Phys.* C **6**, 3679.

Bratkovsky, A. M., Salje, E. K. H., Marais, S. C. & Heine, V. 1994*b* Theory and computer simulation of tweed texture. *Phase Transitions*, **48**, 1.

Bratkovsky, A. M., Salje, E. K. H. & Heine, V. 1994*c* Overview of the origin of tweed texture. *Phase Transitions* **52**, 75.

Bratkovsky, A. M., Salje, E. K. H., Marais, S. C. & Heine, V. 1995 Strain coupling as the dominant interaction in the structural phase transitions mediated by strain. *Phase Transitions* **55**, 79.

Brown, L. M. 1995 Infinitesimal loops and tweed structure. *Czech. J. Phys.* **45**, 893.

Chen, L.-Q., Wang, Y. & Khachaturyan, A. G. 1992 Kinetics of tweed and twin formation during an ordering transition in a substitutional solid solution. *Phil. Mag. Lett.* **65**, 15.

Dattagupta, S., Heine, V., Marais, S. & Salje, E. 1991 A rate-equation for atomic ordering in mean field-theory. 2. General considerations. *J. Phys.* C **3**, 2975.

David, W. I. F., Harrison, W. T. A., Gunn, J. M. F., Moze, O., Soper, A. K., Day, P., Jorgensen, J. D., Hinks, D. G., Beno, M. A. Soderholm, L., Capone, D. W., Schuller, I. K., Segre, C. U., Zhang, K. & Grace, J. D. 1987 Structure and crystal chemistry of the high-T_c superconductor YBa2Cu_3O_{7-x}. *Nature* **327**, 310.

Dove, M. T., Giddy, A. P. & Heine, V. 1992 On the application of mean-field and Landau theory to displacive phase transitions. *Ferroelectrics* **136**, 33.

Dove, M. T., Giddy, A. P. & Heine, V. 1993 Rigid unit modes of displacive phase transitions in framework silicates. *Trans. Am. Cryst. Assoc.* **27**, 65.

Doukhan, J.-C. 1994 Shock-induced crystal-glass transition in solid silica. *Phase Transitions* **48**, 169.

Eshelby, J. D. 1956 Continuum theory of defects. *Solid St. Phys.* **3**, 79.

Etxebarria, I., Perez-Mato, J. M. & Criado, A. 1990 Incommensurate instability and lattice-dynamics of potassium selenate within a semiempirical rigid-ion model. *Phys. Rev.* B **13**, 8482.

Etxebarria, I., Perez-Mato, J. M. & Madariaga, G. 1992 Lattice-dynamics, structural stability, and phase-transitions in incommensurate and commensurate A2BX4 materials. *Phys. Rev.* B **46**, 2764.

Fahy, S. & Merlin, R. 1994 Reversal of ferroelectric domains by ultrashort optical pulses. *Phys. Rev. Lett.* **73**, 1122.

Heine, V., Bratkovsky, A. M. & Salje, E. K. H. 1994 The effect of clamped and free boundaries on long range strain coupling in structural phase transitions. *Phase Tran.* **52**, 85.

Hemley, R. J., Jephcoat, A. P., Mao, H. K., Ming, L. C. & Manghnani, M. H. 1988 Pressure induced amorphization of crystalline silica. *Nature* **334**, 52.

Jorgensen, J. D., Beno, M. A., Hinks, D. G., Soderholm, L., Volin, K. J., Hitterman, R. L., Grace, J. D., Schuller, I. K., Segre, C. U., Zhang, K. & Kleefisch, M. S. 1987 Oxygen ordering and the orthorhombic-to-tetragonal phase transition in $YBa_2Cu_3O_{7-x}$. *Phys. Rev.* B **36**, 3608.

Khachaturyan, A. G. 1983 *Theory of structural transformations in solids.* New York: Wiley.

Landau, L. D. & Khalatnikov, I. M. 1954 On the kinetics of second order phase transitions. *Dokl. Akad. Nauk SSSR* **96**, 469.

Landau, L. D. & Lifschitz, E. M. 1986 *Statistical physics*, part I. New York: Pergamon.

PHILOSOPHICAL TRANSACTIONS OF THE ROYAL SOCIETY A MATHEMATICAL, PHYSICAL & ENGINEERING SCIENCES

Marais, S. & Salje, E. 1991 Derivation of a rate law for nonuniform systems and continuous order parameters. *J. Phys.* C **3**, 3667.

Marais, S., Heine, V., Nex, C. & Salje, E. 1991*a* Phenomena due to strain coupling in phase-transitions. *Phys. Rev. Lett.* **66**, 2480.

Marais, S., Padlewski, S. & Salje, E. 1991*b* On the origin of kinetic rate-equations—Salje-Glauber-Kawasaki *J. Phys.* C **3**, 6571.

Marais, S., Salje, E. & Heine, V. 1991*c* Kinetic rate laws as derived from order parameter theory. 5. Computer-simulations of ordering processes using a soft Ising-model. *Phys. Chem. Min.* **18**, 180.

Marais, S. C., Salje, E. K. H, Heine, V. & Bratkovsky, A. M. 1994 Strain-related microstructures in materials: a computer simulation study of a simple model. *Phase Transitions* **48**, 15.

Masaki, Y., Suzuki, M. & Kitagawa, A. 1995 Transient phases of a-Si by rapid heating. *J. Appl. Phys.* **77**, 1766.

McNeil, L. E. & Grimsditch, M. 1992 Pressure amorphized SiO_2, α quartz: an anisotropic amorphous solid. *Phys. Rev. Lett.* **68**, 83.

Michel, K. H. & Rowe, J. M. 1985 Molecular symmetry and translation-rotation coupling in orientationally disordered crystals. *Phys. Rev.* B **32**, 5818.

Michel, K. H. & Theuns, T. 1989 Structural phase transitions and polymorphism in mixed crystals $M(CN)_xX_{1-x}$ (M = Na, K, Rb; X = Cl, Br, I). *Phys. Rev.* B **40**, 5761.

Miltat, J. E. A. & Kléman, M. 1973 Magnetostrictive displacements around a domain wall junction: elastic field calculation QD application to X-ray topography. *Phil. Mag.* **28**, 523.

Ortiz-Lopez, J. & Luty, F. 1989 Optical studies of thermal cycling and hysteresis effects in elastic order-disorder phase-transformations. 1. Pure alkali-metal cyanide crystals. *Phys. Rev.* B **37**, 5452.

Parlinski, K., Heine, V. & Salje, E. K. H. 1993*a* Origin of tweed texture in the simulation of a cuprate superconductor. *J. Phys.* C **5**, 497.

Parlinski, K., Salje, E. K. H. & Heine, V. 1993*b* Annealing of tweed microstructure in high-T_c superconductors studied by a computer-simulation. *Acta Metall. Mater.* **41**, 839.

Patashinskii, A. Z. & Pokrovskii, V. L. 1979 *Fluctuation theory of phase transitions.* Oxford: Pergamon.

Poulsen, H. F., Andersen, N. H., Andersen, J. V., Bohr, H. & Mouritsen, O. G. 1991 Relation between superconducting transition temperature and oxygen ordering in $YBa_2Cu_3O_{6+x}$. *Nature* **349**, 594.

Powell, B. M. & Gerlach, P. N. 1989 Soft-mode transition in the ferroelastic crystal $K_2Hg(CN)_4$. *Phys. Rev.* B **40**, 2426.

Putnis, A. 1992 *Introduction to mineral science.* Cambridge University Press.

Reyes-Gasga, J., Krekels, T., Van Tendeloo, G., Van Landuyt, J., Amelinckx, S., Bruggink, W. H. M. & Verweij, H. 1989 3D vacancy ordered superstructures in homogeneous $YBa_2Cu_3O_{7-\delta}$. *Physica* **159C**, 831.

Robertson, I. M. & Wayman, C. M. 1983 Tweed microstructures. III. Origin of the tweed contrast in β and γ Ni–Al alloys. *Phil. Mag.* A **48**, 629.

Salje, E. K. H. 1993*a* *Phase transitions in ferroelastic and coelastic crystals.* Cambridge University Press.

Salje, E. K. H. 1993*b* On the kinetics of partially conserved order parameter: a possible mechanism for pattern formation. *J. Phys.* C **5**, 4775–4784.

Salje, E. K. H. & Parlinski, K. 1991 Microstructures in high-T_c superconductors. *Supercond. Sci. Technol.* **4**, 93.

Salje, E. K. H., Kuscholke, B., Wruck, B. & Kroll, H. 1985 Thermodynamics of sodium-feldspar. 2. Experimental results and numerical calculations. *Phys. Chem. Min.* **12**, 99.

Salje, E. K. H., Wruck, B., Graeme-Barber, A. & Carpenter, M. A. 1993 Experimental test of rate equations: time evolution of Al,Si ordering in anorthite $CaAl_2Si_2O_8$. *J. Phys.* C **5**, 2961–2968.

Sapriel, J. 1975 Domain wall orientations in ferroelastics. *Phys. Rev.* B **12**, 5128.

PHILOSOPHICAL TRANSACTIONS OF THE ROYAL SOCIETY A MATHEMATICAL, PHYSICAL & ENGINEERING SCIENCES

Schmahl, W. W., Putnis, A., Salje, E., Freeman, P., Graeme-Barber, A., Jones, R., Singh, K. K., Blunt, J., Edwards, P. P., Loram, J. & Mirza, K. 1989 Twin formation and structural modulations in orthorhombic and tetragonal $YBa_2(Cu_{1-x}Co_x)_3O_{7-\delta}$. *Phil. Mag. Lett.* **60**, 241.

Semenovskaya, S. & Khachaturyan, A. G. 1991 Kinetics of strain-related morphology transformation in $YBa_2Cu_3O_{7-\delta}$. *Phys. Rev. Lett.* **67**, 2223.

Semenovskaya, S. & Khachaturyan, A. G. 1992 Structural transformations in non-stoichiometric $YBa_2Cu_3O_{6+\delta}$. *Phys. Rev.* B **46**, 6511.

Seto, H., Noda, Y. & Yamada, Y. 1990 Precursor phenomena at martensitic phase transitions in Fe-Pd alloy. 2. Diffuse scattering and embryonic fluctuations. *J. Phys. Soc. Japan* **59**, 978.

Tanner, L. E., Pelton, A. R. & Gronsky, R. 1982 The characterization of pretransformation morphologies—periodic strain modulations. *J. Physique* **43**, suppl. 12, C4-169.

Tautz, F. S., Heine, V., Dove, M. T. & Chen, X. J. 1991 Rigid unit modes in the molecular-dynamics simulation of quartz and the incommensurate phase-transition. *Phys. Chem. Min.* **18**, 326.

Tersoff, J. 1995 Enhanced solubility of impurities and enhanced diffusion near crystal surfaces. *Phys. Rev. Lett.* **74**, 5080.

Tsatskis, I., Salje, E. K. H. & Heine, V. 1994 Pattern formation during phase transitions: Kinetics of partially conserved order parameter and the role of gradient energies. *J. Phys.* C **6**, 11 027.

Tsatskis, I. & Salje, E. K. H. 1996 Time evolution of pericline twin domains in alkali feldspars: a computer simulation study. *Am. Mineral.* **81**, 800.

Tsuji, K., Katayama, Y., Koyama, N., Yamamoto, Y., Chen, J. Q. & Imai, M. 1993 Amorphization from quenched high-pressure phase in tetrahedrally bonded materials. *J. Non-Cryst. Sol.* **156**, 540.

Vallade, M., Berge, B. & Dolino, G. 1992 Origin of the incommensurate phase of quartz. 2. Interpretation of inelastic neutron-scattering data. *J. Physique* **2**, 1481.

Van Tendeloo, G., Zandbergen, H. W. & Amelinckx, S. 1987 Electron-diffraction and electron-microscopic study of Ba–Y–Cu–O superconducting materials. *Solid St. Commun.* **63**, 389.

Vaks, V. G., Larkin, A. I. & Pikin, S. A. 1966 On the self-consistent field method for description of phase transitions. *Zh. Eksp. Teor. Fiz.* **51**, 361–375 (*Sov. Phys. JETP* **51**, 240).

Wen, S. H., Khachaturyan, A. G. & Morris, J. W. 1981 Computer-simulation of a tweed-transformation in an idealised elastic crystal. *Metall. Trans.* A **12**, 581.

Zener, C. 1948 Theory of strain interaction of solute atoms. *Phys. Rev.* **74**, 639.

Zhu, Y., Suenaga, M. & Tafto, J. 1991 Multiple diffuse scattering and tweed contrast in $YBa_2Cu_3O_{7-\delta}$. *Phil. Mag. Lett.* **64**, 29.

PHILOSOPHICAL TRANSACTIONS OF THE ROYAL SOCIETY A MATHEMATICAL, PHYSICAL & ENGINEERING SCIENCES

(a)

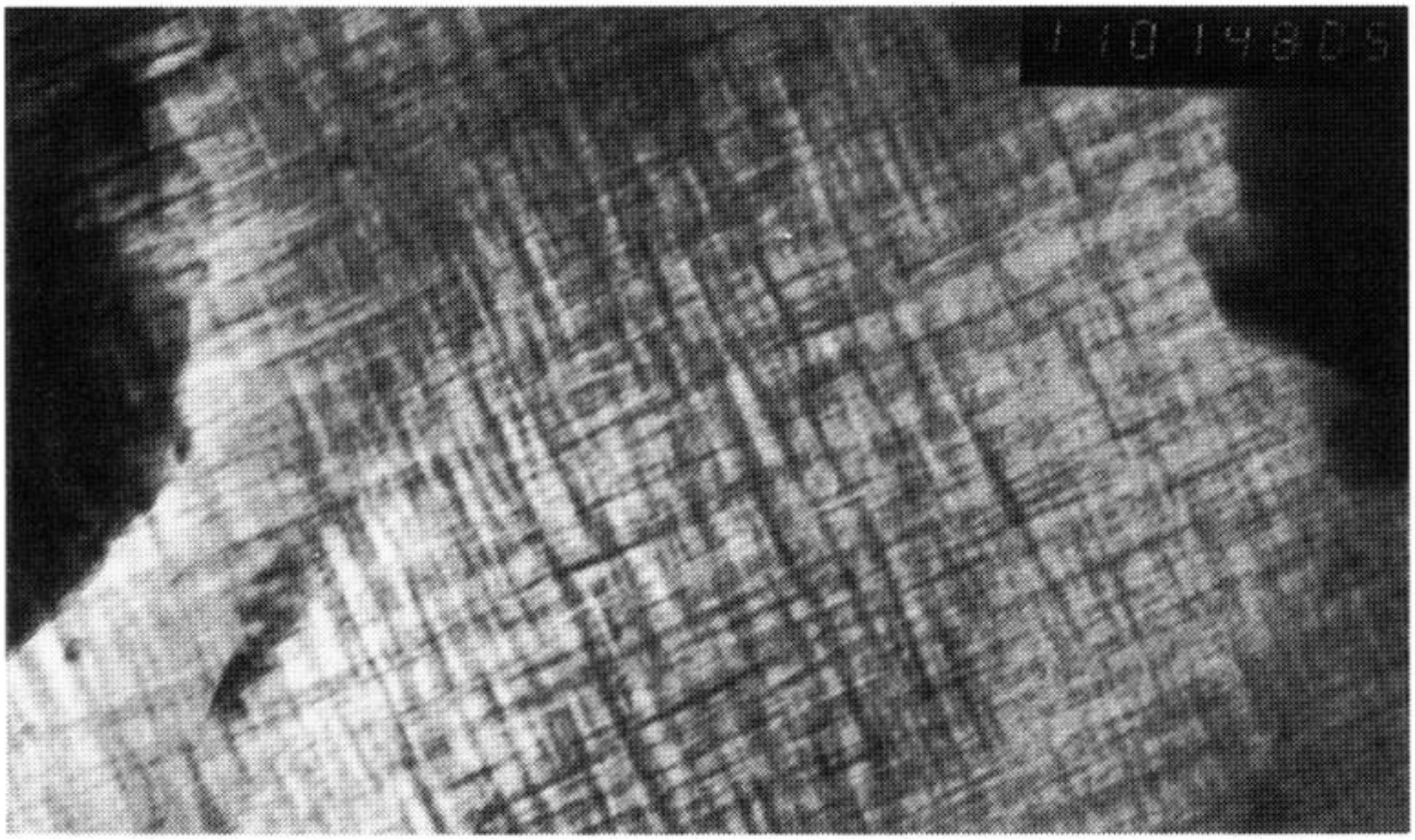

(b)

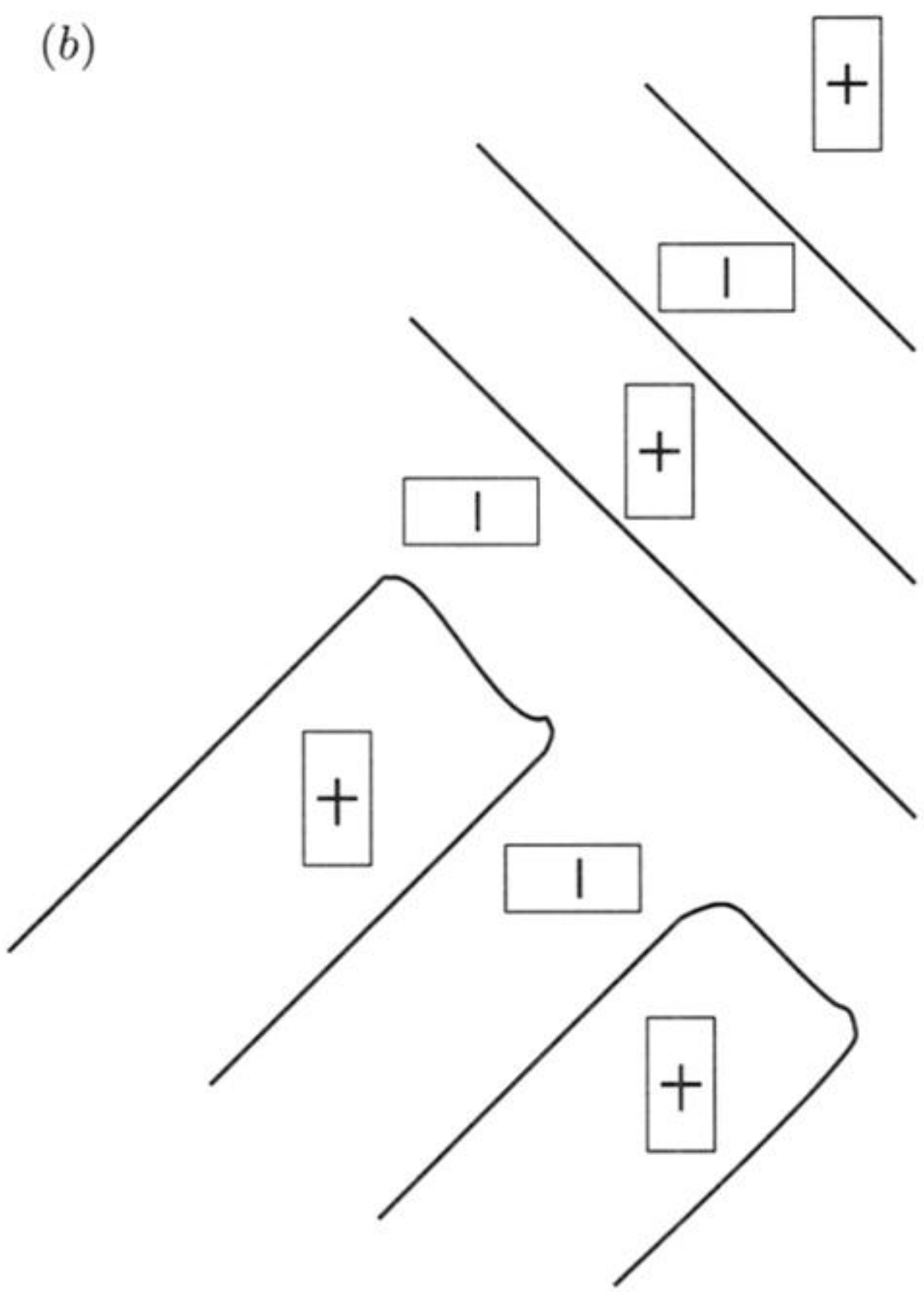

PHILOSOPHICAL TRANSACTIONS OF THE ROYAL SOCIETY A MATHEMATICAL, PHYSICAL & ENGINEERING SCIENCES

igure 2. (*a*) Microstructure of Co-doped $YBa_2(Cu,Co)_3O_7$. Scale: the black label insert is 2 μm long (photograph by courtesy of A. Putnis, Cambridge). (*b*) Tweed texture in Co-doped BCO (schematic). The domains with opposite spontaneous strains are shown to form a char-teristic cross-hatched domain pattern.

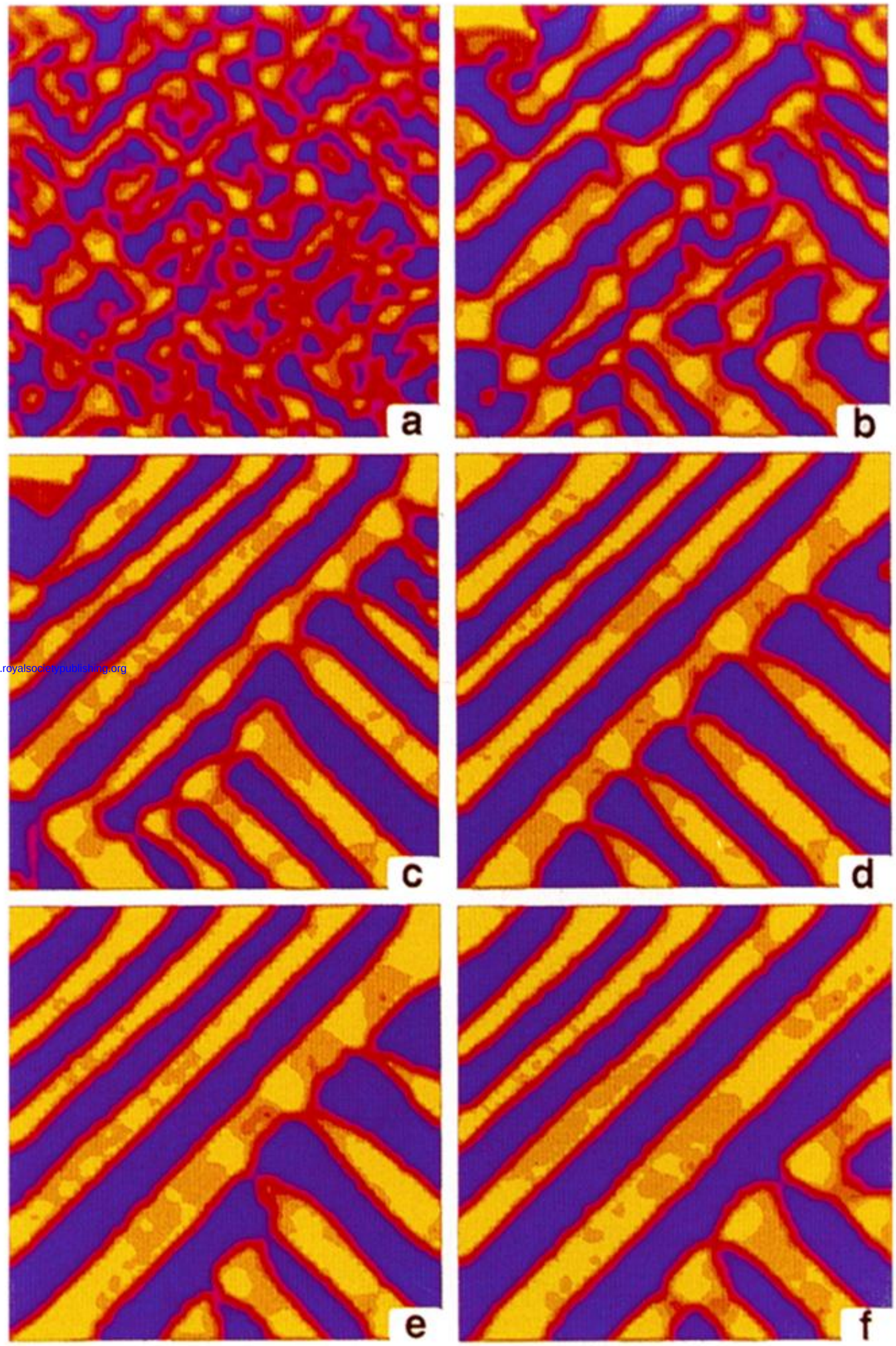

gure 8. The maps of strain order parameter obtained during annealing at temperature
$= 0.43T_c$ after quenching from $T = 2T_c$. Those from (a)–(f) correspond to annealing time
= 10, 50, 200, 1000, 2000 and 4000 Monte Carlo steps per site. Note the immediate appearance
tweed in (a) due to the pre-existence of embryos at $2T_c$, the sharpening up of microdomain
alls in (b), the coarsening in (b), (c), and the formation of needle domains in (d)–(f).

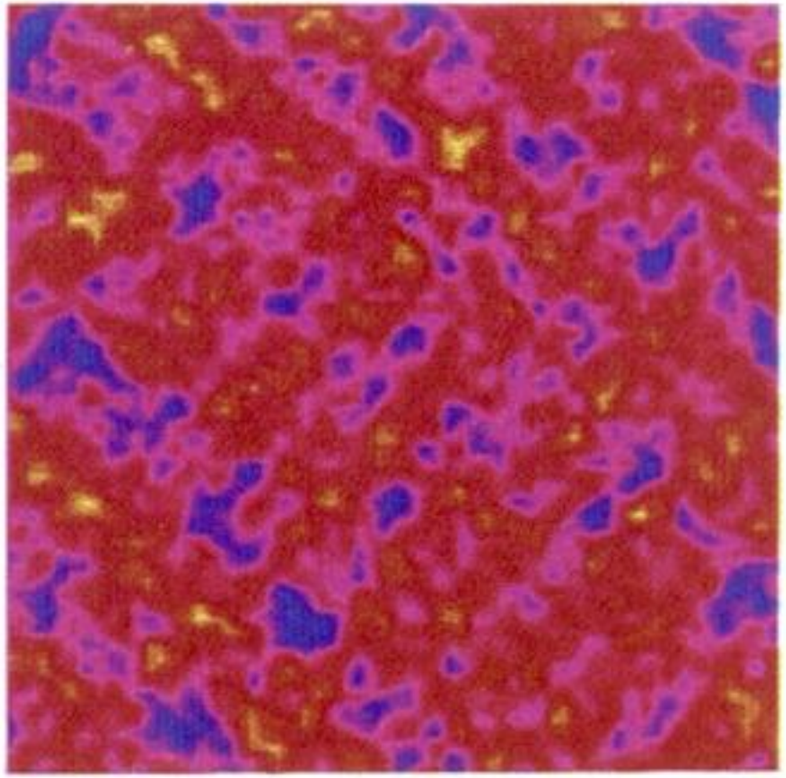

gure 10. The map of the strain order parameter at temperature $1.3T_c$ showing the embryonic
ıctuations for a system with e_{xx}–e_{yy} type of coupling and boundaries of the type in figure 2*c*.

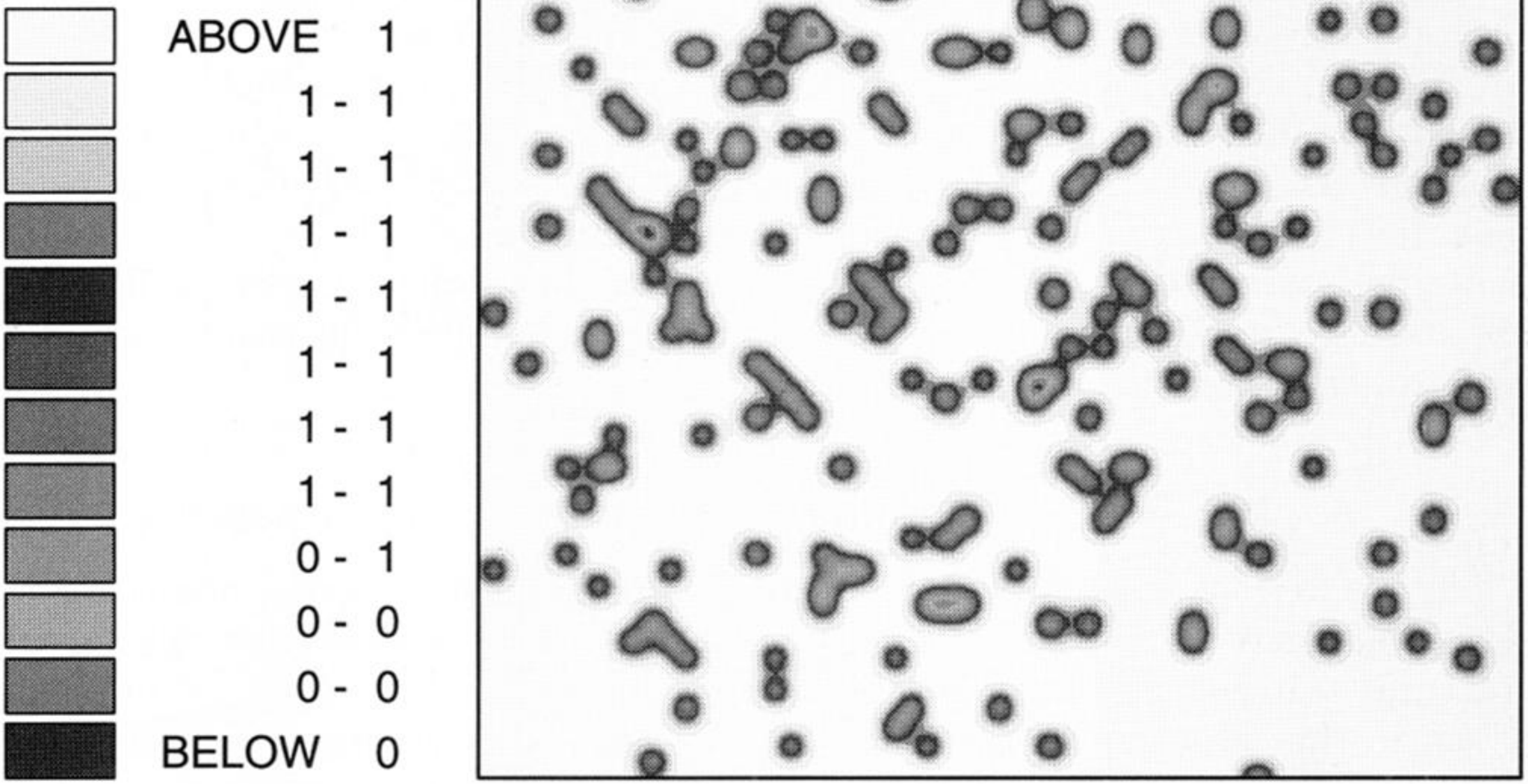

igure 12. Sudden heating: model system which has initially been set in state with all $Q_i = 1$ nd then subjected to instant heating to $0.4T_c$. (a) After $t = 2$ Monte Carlo steps a few spins ave flipped in rather random manner.

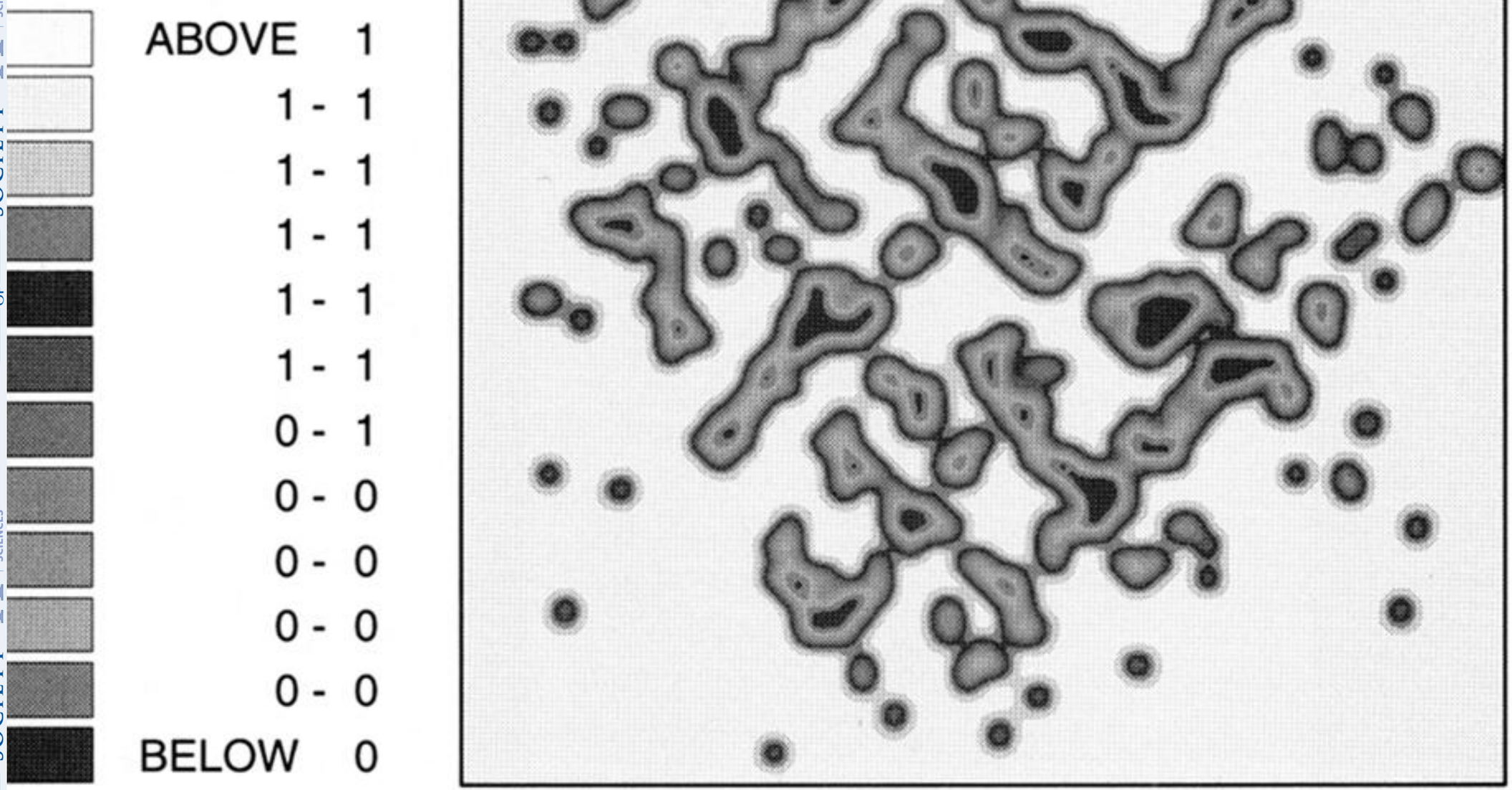

Figure 12. *Cont.* (*b*) After $t = 50$ Monte Carlo steps the long range elastic interaction between ordering variables resulted in tweed.